An essential cell-autonomous role for hepcidin in cardiac iron homeostasis

Samira Lakhal-Littleton[1*], Magda Wolna[1], YuJin Chung[1], Helen C Christian[1], Lisa C Heather[1], Marcella Brescia[1], Vicky Ball[1], Rebecca Diaz[2], Ana Santos[2], Daniel Biggs[2], Kieran Clarke[1], Benjamin Davies[2], Peter A Robbins[1]

1 Department of Physiology, Anatomy and Genetics, University of Oxford. Parks Road, Oxford OX1 3PT

2 Wellcome Trust Centre for Human Genetics, University of Oxford. Roosevelt Drive, Oxford, OX3 7BN.

*To whom correspondence should be addressed. Tel: +441865272543. Email:samira.lakhal-littleton@dpag.ox.ac.uk

ABSTRACT

Hepcidin is the master regulator of systemic iron homeostasis. Derived primarily from the liver, it inhibits the iron exporter ferroportin in the gut and spleen, the sites of iron absorption and recycling respectively. Recently, we demonstrated that ferroportin is also found in cardiomyocytes, and that its cardiac-specific deletion leads to fatal cardiac iron overload. Hepcidin is also expressed in cardiomyocytes, where its function remains unknown. To define the function of cardiomyocyte hepcidin, we generated mice with cardiomyocyte-specific deletion of hepcidin, or knock-in of hepcidin-resistant ferroportin. We find that while both models maintain normal systemic iron homeostasis, they nonetheless develop fatal contractile and metabolic dysfunction as a consequence of cardiomyocyte iron deficiency. These findings are the first demonstration of a cell-autonomous role for hepcidin in iron homeostasis. They raise the possibility that such function may also be important in other tissues that express both hepcidin and ferroportin, such as the kidney and the brain.

INTRODUCTION

As a constituent of hemoproteins, iron-sulphur proteins and other functional groups, iron is essential for cellular functions. Conversely, excess iron participates in cytotoxic Fenton-type chemical reactions. Thus, both iron deficiency and iron overload are detrimental to the cell. Therefore, the healthy functioning of tissues requires tight control of intracellular iron levels. These in turn are dependent both on cellular homeostatic pathways controlling iron uptake, usage, and storage, and on systemic pathways controlling iron levels in the plasma. In mammals, cellular iron homeostasis is controlled by the Iron Regulatory Proteins IRPs. Intracellular iron levels control the degradation of IRP2 and the conformational switch that confers the RNA-binding function of IRP1. IRPs in turn control the levels of iron uptake proteins such as transferrin receptor 1 (TfR1) and divalent metal transporter (DMT1), and the iron storage protein ferritin (1,2). Systemic iron homeostasis is controlled by the hepcidin/ferroportin axis at the sites of iron entry into the circulation. Ferroportin (FPN), which is encoded by the Solute Carrier Family 40 Member 1 (*Slc40a1*), is the only known mammalian iron export protein and mediates iron release into the circulation from duodenal enterocytes, splenic reticuloendothelial macrophages and hepatocytes, the sites of iron absorption, recycling and storage respectively (3,4). FPN-mediated iron release is antagonized by the hormone hepcidin, also known as hepcidin antimicrobial peptide (HAMP). Produced primarily in the liver, hepcidin binds to and induces internalization of FPN, thereby limiting iron release into the circulation and its availability to peripheral tissues (5,6). The importance of the HAMP/FPN axis is illustrated by diseases of systemic iron overload such as hemochromatosis and β-thalassaemia, where hepcidin production is impaired (7,8), and in anaemia of chronic disease where hepcidin production is inappropriately elevated (9,10).

Other than the liver, hepcidin is also found in tissues with no recognized role in systemic iron homeostasis, including the heart (11), the brain (12), the kidney (13) and the placenta (14). The function of this extra-hepatic hepcidin remains unknown, but one hypothesis is that it is involved in local iron control. Relevant to this hypothesis are our recent findings that FPN is

also present in the heart, that it is essential for cardiomyocyte iron homeostasis and that its cardiomyocyte-specific deletion leads to fatal cardiac iron overload in mice (15). Therefore, we hypothesised that cardiac HAMP regulates cardiac FPN, and that such regulation is important for local iron control and for cardiac function.

To test this hypothesis, we generated two novel mouse models; the first with a cardiomyocyte-specific deletion of the *Hamp* gene, and the second, with cardiomyocyte-specific knock-in of *Slc40a1 C326Y*, that encodes a FPN with intact iron export function but impaired HAMP binding (16,17). We studied cardiac function and iron homeostasis longitudinally in both models and report that both develop fatal cardiac dysfunction and metabolic derangement as a consequence of cardiomyocyte iron deficiency. This occurs against a background of otherwise normal systemic iron homeostasis. Both cardiac dysfunction and metabolic derangement are prevented by intravenous iron supplementation.

Our findings demonstrate that, at least in the cardiomyocyte, endogenously-derived HAMP plays an essential role in cellular, rather than systemic iron homeostasis. It does this through the autocrine regulation of cardiomyocyte FPN. Disruption of this cardiac HAMP/FPN leads to fatal cardiac dysfunction.

Currently, there is considerable clinical interest in strategies that target the HAMP/FPN axis for the treatment of systemic iron overload and iron deficiency. Our findings suggest that these strategies may additionally alter cardiac iron homeostasis and function. Other than the heart, both HAMP and FPN are also found in the brain, kidney and placenta (12,13,14, 18, 19, 20, 21). A pertinent question is the extent to which our findings in the heart extend to those tissues.

RESULTS

Hamp expression and regulation in the heart

Hamp mRNA levels were approximately 30 fold lower in the adult mouse heart than in the liver (Figure 1a). Next, we examined the regulation of cardiac Hamp mRNA and HAMP protein in response to dietary iron manipulation, having first established that this dietary

manipulation altered cardiac and liver iron levels (Figure 1- Figure Supplement 1). In both tissues, Hamp mRNA levels were decreased by the iron-deficient diet (Fe 2-5ppm) and increased by the iron-loaded diet (Fe 5000ppm)(Figure 1a). At the protein level, while changes in hepatic HAMP protein mirrored changes in its mRNA levels, cardiac HAMP protein was increased by the iron-deficient diet and unaffected by the iron-loaded diet (Figure 1b).

To explore further the regulation of cardiac hepcidin by iron, we isolated primary adult cardiomyocytes from mice, then carried out a timecourse treatment with the iron chelator desferroxamine DFO, or with ferric citrate FAC. Under control conditions, Hamp mRNA was upregulated following addition of fresh cardiomyocyte culture medium (cardiomyocytes are cultured for 2 hours in serum-free medium prior to this). Relative to control cardiomyocytes at the respective timepoint, Hamp mRNA was increased by FAC from 4 hours of treatment, and decreased by DFO at 4, 8 and 16 hours of treatment (Figure 1c). HAMP protein, measured by ELISA in supernatants was also increased following addition of fresh medium. Relative to control cardiomyocytes at the respective timepoint, HAMP protein in supernatants was increased by DFO as early as 2 hours, but remained unchanged by FAC at all timepoints (Figure 1d). Thus, the direction of response of the Hamp mRNA and HAMP protein to iron levels *in vitro* mirrored the responses seen *in vivo*.

Next, we aimed to understand the mechanisms underlying increased HAMP secretion in DFO-treated cardiomyocytes. To this end, we investigated the role of the prohormone convertase Furin, which in hepatocytes, is required for cleavage of the propeptide and the release of the mature HAMP peptide (22). Furin expression has been reported in the heart (23, 24), and we also found that its expression was upregulated in the hearts of mice provided an iron-deficient diet and in cardiomyocytes treated with DFO (Figure 1- Figure Supplement 2). When we measured HAMP in supernatants of cardiomyocytes treated with the Furin inhibitor decanoyl-Arg-Val-Lys-Arg-chloromethylketone (CMK), we found no increase in HAMP release following DFO treatment (Figure 1d). We confirmed that Hamp mRNA levels in cardiomyocytes were not altered by CMK treatment (Figure 1- Figure

Supplement 3). Together, these results indicate that Furin upregulation mediates increased HAMP secretion from iron-deficient cardiomyocytes.

Having established that hepcidin is found in cardiomyocytes, we then aimed to define its function. To this end, we generated cardiomyocyte-specific *Hamp* knockout mice *Hamp*$^{fl/fl}$;*Myh6.Cre*+ by crossing in-house conditional *Hamp* floxed (fl) mice with mice transgenic for Cre recombinase under the control of cardiomyocyte-specific promoter Myosin Heavy Chain 6 (*Myh6.Cre*+). Hamp mRNA (Figure 1e) and HAMP protein (Figure 1f) in the hearts of *Hamp*$^{fl/fl}$;*Myh6.Cre*+ mice were significantly reduced compared to the hearts of *Hamp*$^{fl/fl}$ controls. Furthermore, compared to *Hamp*$^{fl/fl}$ cardiomyocytes, levels of HAMP protein in the supernatants of cardiomyocytes from *Hamp*$^{fl/fl}$;*Myh6.Cre*+ mice were either greatly reduced or undetectable, both under baseline conditions and following treatment with DFO or FAC (Figure 1- Figure Supplement 4). Near complete ablation of the cardiac Hamp mRNA and HAMP protein in *Hamp*$^{fl/fl}$;*Myh6.Cre*+ mice confirmed that cardiomyocytes were the primary site of hepcidin expression in the heart. Liver Hamp mRNA (Figure 1e) and HAMP protein (Figure 1f) were not different between *Hamp*$^{fl/fl}$;*Myh6.Cre*+ and *Hamp*$^{fl/fl}$ controls, consistent with the cardiac-specific nature of *Hamp* gene deletion.

Also consistent with this cardiac-specific deletion, *Hamp*$^{fl/fl}$;*Myh6.Cre*+ mice had normal levels of liver iron stores and circulating markers of iron homeostasis when compared to *Hamp*$^{fl/fl}$ controls, demonstrating that loss of cardiac hepcidin did not affect systemic iron homeostasis. In addition, circulating HAMP levels were not reduced in the serum of *Hamp*$^{fl/fl}$;*Myh6.Cre*+ mice, suggesting that cardiac hepcidin does not contribute significantly to circulating HAMP levels (Table 1).

Fatal cardiac abnormalities in *Hamp*$^{fl/fl}$;*Myh6.Cre*+ mice

To determine the effects of loss of cardiac hepcidin, we first assessed the cumulative survival of *Hamp*$^{fl/fl}$;*Myh6.Cre*+ mice and *Hamp*$^{fl/fl}$ littermate controls over a period of 52 weeks. Significantly greater mortality was observed amongst *Hamp*$^{fl/fl}$;*Myh6.Cre*+ mice, with only 29% of animals surviving to 52 weeks, compared with 90% of *Hamp*$^{fl/fl}$ controls. The

137 median survival of *Hamp*$^{fl/fl}$;*Myh6.Cre*+ mice was 28 weeks, whereas the majority of *Hamp*$^{fl/fl}$
138 controls were still alive at 52 weeks (Figure 2a).
139 Six-month old mice were sacrificed for assessment of cardiac morphology, which showed
140 gross enlargement of the left ventricle (LV) in *Hamp*$^{fl/fl}$;*Myh6.Cre*+ hearts compared to
141 *Hamp*$^{fl/fl}$ controls (Figure 2b). Assessment of cardiomyocyte size by wheat germ agglutinin
142 (WGA) staining confirmed that *Hamp*$^{fl/fl}$;*Myh6.Cre*+ cardiomyocytes were hypertrophied
143 (Figure 2c-d). This was accompanied by upregulation of expression of hypertrophic gene
144 markers myosin heavy chain (*Myh7)* and natriuretic peptide precursor *(Nppb)* (Figure 2e).
145 TUNEL staining for *in-situ* detection of cell death also showed significantly greater apoptosis
146 in the hearts of *Hamp*$^{fl/fl}$;*Myh6.Cre*+ mice than in *Hamp*$^{fl/fl}$ controls (Figure 2f-g).
147 To characterise further the phenotype caused by loss of cardiac hepcidin, we used cine MRI
148 in anaesthetised *Hamp*$^{fl/fl}$;*Myh6.Cre*+ mice and *Hamp*$^{fl/fl}$ littermate controls at 3, 6 and 9
149 months of age. Mid-ventricular cine MR images showed no differences between the two
150 genotypes at 3 months of age. At 6 and 9 months of age, cine MR images showed marked
151 enlargement of the LV in *Hamp*$^{fl/fl}$;*Myh6.Cre*+ mice compared to *Hamp*$^{fl/fl}$ controls (Figure
152 2h). Formal quantitation of cardiac parameters by cine MRI confirmed enlargement of the LV
153 lumen in *Hamp*$^{fl/fl}$;*Myh6.Cre*+ mice, both at end-systole (LVES) (Figure 2i) and at end-
154 diastole (LVED) (Figure 2j), accompanied by a decrease in LV ejection fraction (LVEF) from
155 62% to 42% (Figure 2k). Other parameters of cardiac performance were not significantly
156 altered between mice from the two genotypes (Table 2). Taken together, histological
157 examination of the hearts and cine MRI studies indicated that *Hamp*$^{fl/fl}$;*Myh6.Cre*+ mice
158 developed fatal LV dysfunction with reduced LVEF.
159 Such changes in cardiac performance could not be attributed to Cre recombinase toxicity in
160 the heart as we have previously shown that *Myh6.Cre*+ mice have normal cardiac function
161 compared to wild type littermate controls (15).
162 **The role of cardiomyocyte FPN in the phenotype of *Hamp*$^{fl/fl}$;*Myh6.Cre*+ mice**
163 We examined FPN protein in the hearts of *Hamp*$^{fl/fl}$;*Myh6.Cre*+ mice, and found that FPN
164 protein was markedly upregulated compared to *Hamp*$^{fl/fl}$ controls (Figure 3a), consistent with

the idea that loss of cardiac HAMP was acting through upregulation of cardiomyocyte FPN. In order to test whether cardiac dysfunction arose from upregulation of cardiomyocyte FPN, we engineered mice where the *Slc40a1* gene harbours a conditional cardiac-specific C326Y point mutation, which confers HAMP-resistance while conserving the iron export function of FPN (16,17). We confirmed that the *Slc40a1 C326Y* fl allele produced the C326Y transcript specifically in the heart (Figure 3- Figure Supplement 1) and that *Slc40a1 C326Y*$^{fl/fl}$;*Myh6.Cre*+ mice did not exhibit changes in systemic iron indices (Table 3). As seen in *Hamp*$^{fl/fl}$;*Myh6.Cre*+ mice, cardiomyocyte FPN was indeed upregulated in *Slc40a1 C326Y*$^{fl/fl}$;*Myh6.Cre*+ mice (Figure 3b).

Like *Hamp*$^{fl/fl}$;*Myh6.Cre*+ mice, *Slc40a1 C326Y*$^{fl/fl}$;*Myh6.Cre*+ mice also had increased mortality relative to their littermate controls (Figure 3c). We then determined whether *Slc40a1 C326Y*$^{fl/fl}$;*Myh6.Cre*+ mice developed the same phenotype of cardiac dysfunction as *Hamp*$^{fl/fl}$;*Myh6.Cre*+ mice. Histologically, *Slc40a1 C326Y*$^{fl/fl}$;*Myh6.Cre*+ hearts from 6 month old mice also showed LV enlargement (Figure 3d), hypertrophied cardiomyocytes (Figure 3e-f), upregulation of hypertrophy markers *Myh7* and *Nppb* (Figure 3g) and a greater degree of apoptosis compared to *Slc40a1 C326Y*$^{fl/fl}$ controls (Figure 3h-i). When we measured cardiac performance by cine MRI, we found that *Slc40a1 C326Y*$^{fl/fl}$;*Myh6.Cre*+ mice also developed LV dysfunction by 6 months of age, with a reduction in LVEF from 73% to 55% (Figure 3j-l).

The similarity between *Hamp*$^{fl/fl}$;*Myh6.Cre*+ and *Slc40a1 C326Y*$^{fl/fl}$;*Myh6.Cre*+ mice in terms of the nature and time course of cardiac dysfunction suggests a common mechanism of cardiac dysfunction involving upregulation of cardiomyocyte FPN. Therefore, we tested whether this upregulation of FPN resulted in increased iron efflux from cardiomyocytes. Iron Fe55 efflux was indeed significantly greater in cardiomyocytes isolated from *Hamp*$^{fl/fl}$;*Myh6.Cre*+ and *Slc40a1 C326Y*$^{fl/fl}$;*Myh6.Cre*+ hearts than in cardiomyocytes isolated from their respective controls (Figure 3m). Addition of exogenous mouse HAMP in the efflux medium inhibited the increase in Fe55 efflux from *Hamp*$^{fl/fl}$;*Myh6.Cre*+ cardiomyocytes but not from *Slc40a1 C326Y*$^{fl/fl}$;*Myh6.Cre*+ cardiomyocytes, consistent with

the HAMP-resistant mutation in *Slc40a1 C326Y*$^{fl/fl}$;*Myh6.Cre*+ cardiomyocytes. We hypothesised that upregulation of cardiac FPN and iron export in *Hamp*$^{fl/fl}$;*Myh6.Cre*+ and *Slc40a1 C326Y*$^{fl/fl}$;*Myh6.Cre*+ hearts caused cardiomyocyte iron depletion. To test this hypothesis, we quantified iron levels both in total hearts and in the isolated cardiomyocyte fractions at 3 months and 6 months of age. While iron levels in total hearts were not significantly different between any of the genotypes (Figure 3- Figure Supplement 2), the iron content of the cardiomyocyte fraction was significantly lower in *Hamp*$^{fl/fl}$;*Myh6.Cre*+ and in *Slc40a1 C326Y*$^{fl/fl}$;*Myh6.Cre*+ mice than in their respective controls (Figure 3n). Furthermore, expression of TfR1 mRNA was upregulated (Figure 3o) and Slc40a1 mRNA was downregulated (Figure 3p) in *Hamp*$^{fl/fl}$;*Myh6.Cre*+ and *Slc40a1 C326Y*$^{fl/fl}$;*Myh6.Cre*+ hearts relative to their respective controls, consistent with a transcriptional response to intracellular iron deficiency (1,2,25). Together these results demonstrate that loss of either cardiac hepcidin or hepcidin responsiveness in the heart results in upregulation of cardiomyocyte FPN, and that cardiomyocytes of *Hamp*$^{fl/fl}$;*Myh6.Cre*+ and *Slc40a1 C326Y*$^{fl/fl}$;*Myh6.Cre*+ hearts are iron deficient as a result of upregulation of FPN-mediated iron export.

The role of cardiomyocyte iron deficiency and metabolic derangement in cardiac dysfunction

As cardiomyocyte iron deficiency preceded the development of cardiac dysfunction, we hypothesised it is the cause of the cardiac phenotype in *Hamp*$^{fl/fl}$;*Myh6.Cre*+ mice. To test this hypothesis, we treated *Hamp*$^{fl/fl}$;*Myh6.Cre*+ mice and *Hamp*$^{fl/fl}$ controls with fortnightly intravenous injections of ferric carboxymaltose solution containing 0.5mg iron from 3 months of age, and confirmed the effects of this treatment on cardiac and systemic iron indices at 6 months of age (Table 4). At this timepoint, we performed cine MRI and found that the LV enlargement and the reduced LVEF, seen in untreated *Hamp*$^{fl/fl}$;*Myh6.Cre*+ mice, were prevented in iron-treated *Hamp*$^{fl/fl}$;*Myh6.Cre*+ mice (Figure 4a-c). The transcriptional response to intracellular iron deficiency in untreated *Hamp*$^{fl/fl}$;*Myh6.Cre*+ mice (upregulation of TfR1 mRNA and downregulation of Slc40a1 mRNA relative to *Hamp*$^{fl/fl}$ controls), was absent in iron-treated *Hamp*$^{fl/fl}$;*Myh6.Cre*+ mice, consistent with correction of cardiomyocyte

iron deficiency (Figure 4d-e). Prevention of cardiac dysfunction in *Hamp*$^{fl/fl}$;*Myh6.Cre*+ mice by intravenous iron treatment confirms the causal relationship between cardiomyocyte iron deficiency and cardiac dysfunction in this setting.

Having confirmed a causal relationship between cardiomyocyte iron deficiency and cardiac dysfunction, we aimed to understand the mechanisms linking the two. Iron is a cofactor for several enzymes involved in metabolism (26,27,28), and metabolic derangement is a well-recognized precursor to cardiac dysfunction (29,30,31). Iron deficiency has been reported to reduce the levels and/or activities of key metabolic iron-containing enzymes, in cell lines, in the hearts of mice with impaired cardiac iron uptake (cardiac-specific *TfR1* knockouts) and in the hearts of mice fed an iron-deficient diet (32,33,34,35). Based on those studies, we postulated that iron deficiency in the cardiomyocytes of *Hamp*$^{fl/fl}$;*Myh6.Cre*+ mice would also result in reduction in the activities of key metabolic iron-containing enzymes. To test this hypothesis, we measured the activities of the iron-sulphur containing enzyme Aconitase I as well as electron transport chain (ETC) complexes in cardiac lysates from *Hamp*$^{fl/fl}$;*Myh6.Cre*+ hearts at 3 months and 6 months of age. We found that Aconitase I, Complex I and Complex IV activities were significantly reduced in *Hamp*$^{fl/fl}$;*Myh6.Cre*+ hearts compared to *Hamp*$^{fl/fl}$ controls at 3 months and 6 months of age, and that this reduction in activity was prevented in iron-treated 6-month old mice (Figure 4f-h). As ETC activity is essential to mitochondrial function, we examined whether *Hamp*$^{fl/fl}$;*Myh6.Cre*+ hearts had signs of mitochondrial failure, and whether such mitochondrial failure was prevented by intravenous iron supplementation. By electron microscopy (EM), dilation of mitochondrial cristae was seen in *Hamp*$^{fl/fl}$;*Myh6.Cre*+ hearts as early as 3 months of age and progressed further at 6 months of age. However, this was prevented in iron-treated *Hamp*$^{fl/fl}$;*Myh6.Cre*+ mice, which had healthy-looking mitochondria at 6 months of age (Figure 4i). Similar changes in mitochondrial morphology were seen in the hearts of 3 month old *Slc40a1 C326Y*$^{fl/fl}$;*Myh6.Cre*+ mice (data not shown).

Impairment of electron transport is known to drive glycolysis, as an alternative route of ATP production (36,37). Therefore, we examined the expression of a number of genes encoding

glycolytic enzymes. We found that expression of genes encoding Hexokinase 2 (*Hk2*) which catalyses the first step of glycolysis, Enolase (*Eno*), which catalyses the penultimate step of glycolysis and of Lactate dehydrogenase A (*Ldha)* which catalyses the ultimate step of glycolysis were all significantly increased at 3 months and 6 months of age in hearts of untreated *Hamp*$^{fl/fl}$;*Myh6.Cre+* mice. This upregulation of glycolytic genes was not seen in iron-treated *Hamp*$^{fl/fl}$;*Myh6.Cre+* mice (Figure 4j-l). These results demonstrate that reduction in the activities of key iron-containing metabolic enzymes, mitochondrial failure and upregulated glycolysis precede the development of cardiac dysfunction in *Hamp*$^{fl/fl}$;*Myh6.Cre+* hearts, and are prevented by intravenous iron treatment.

DISCUSSION

The major finding of this study is that cardiomyocyte hepcidin is required for autonomous cellular iron homeostasis. Loss of hepcidin responsiveness specifically in cardiomyocytes engendered the same effects as loss of cardiac hepcidin, demonstrating that cardiac hepcidin operates in an autocrine fashion by regulating cardiomyocyte FPN. A role in cellular iron homeostasis, and an autocrine mode of action for the HAMP/FPN axis have not been described previously in any other tissue. Indeed, hepcidin and FPN are better known to interact in an endocrine fashion, at the level of the gut, spleen and liver, to regulate systemic iron homeostasis.

A second important finding is that this cardiac HAMP/FPN axis is essential for normal heart function, and that its disruption leads to ultimately fatal cardiac metabolic and contractile dysfunction, even against a background of intact systemic iron homeostasis. Metabolic and contractile dysfunction are preceded by cardiomyocyte iron deficiency and prevented by intravenous iron supplementation, indicating a causal relationship between cardiomyocyte iron deficiency and cardiac dysfunction. This causal relationship has previously been demonstrated in studies using mice lacking cardiac TfR1, in which cardiac iron deficiency also affects the heart against a background of otherwise intact systemic iron homeostasis (34). Furthermore, the importance of metabolic derangement seen in our mouse models is

277 also consistent with the findings in mice lacking the cardiacTfR1, and in mice and rats fed
278 iron deficient diets (33,34,38,39). Correction of metabolic and contractile dysfunction by
279 intravenous iron treatment likely involves not only increased iron availability for uptake into
280 cardiomyocytes, but also the effects of increased circulating HAMP on cardiomyocyte FPN.
281 Surprisingly, we found that, both *in vitro* and *in vivo*, cardiac HAMP protein responded
282 differently from its transcript to changes in iron levels. The current understanding of hepcidin
283 regulation is based on studies of hepatic hepcidin. In that setting, release of the active
284 mature HAMP peptide is dependent on cleavage of the propeptide by Furin (22). We found
285 that Furin inhibition increased iron export from *Hamp*$^{fl/fl}$ but not from *Hamp*$^{fl/fl}$;*Myh6.Cre+*
286 cardiomyocytes (Appendix figure 1), demonstrating that cardiomyocytes secrete an active
287 HAMP peptide in a Furin-dependent manner. Furthermore, we found that increased HAMP
288 release from iron-deficient cardiomyocytes depended on Furin, and that cardiac Furin itself is
289 upregulated by iron deficiency both *in vitro* and *in vivo*. The latter finding is consistent with
290 the reported regulation of Furin by iron deficiency through Hypoxia-Inducible Factors HIFs
291 (40). These data suggest that differential regulation of Furin by iron may explain the
292 divergent effects of iron on Hamp transcript and HAMP protein. Comprehensive studies
293 using cardiac-specific knockouts of putative regulators will be required to explore formally
294 the regulation or otherwise, of cardiac hepcidin by pathways known to regulate hepatic
295 hepcidin.
296 The upregulation of cardiac HAMP in mice fed an iron-deficient diet raises the possibility that
297 it may be involved in protecting the heart in the setting of systemic iron deficiency. This
298 hypothesis is supported by the finding that, when provided an iron-deficient diet,
299 *Hamp*$^{fl/fl}$;*Myh6.Cre+* mice exhibited a greater cardiac hypertrophic response than their
300 *Hamp*$^{fl/fl}$ littermate controls (Appendix figure 2).
301 Intracellular iron levels are dependent both on cellular homeostatic pathways and on
302 systemic iron availability in plasma. Therefore, the interplay between the cardiac and the
303 systemic HAMP/FPN axes is important in determining cardiomyocyte iron levels. Some
304 insight into this interplay is gained from comparing systemic and cardiac mouse models of

disrupted iron homeostasis. It is interesting that ubiquitous *Hamp* knockout (15) and ubiquitous *Slc40a1 C326Y* knock-in mice (Appendix figure 3), both models of systemic iron overload, do not develop the cardiac dysfunction seen in cardiomyocyte-specific *Hamp* knockout and cardiomyocyte-specific *Slc40a1 C326Y* knock-in mice. This suggests that, while upregulation of cardiomyocyte FPN under conditions of normal iron availability (cardiac-specific models described in this study) is detrimental to cardiac function, it is protective under conditions of increased systemic iron availability (systemic models). Previously, we also showed that deletion of cardiomyocyte FPN resulted in fatal cardiomyocyte iron overload, preventable by dietary iron restriction (15). Together, our studies demonstrate that iron levels within cardiomyocytes are a balance between cellular iron efflux which is regulated by the cardiac HAMP/FPN axis, and systemic iron availability which is regulated by the systemic HAMP/FPN axis (Figure 5).

Iron overload is detrimental to cardiac health, as demonstrated by iron overload cardiomyopathy in hemochromatosis and thalassemia major patients (41). Our model of cardiac iron homeostasis implies that the cardiac HAMP/FPN axis may have a modifying effect on the severity of iron-overload cardiomyopathy. Thus, it would be interesting to explore whether differences in the levels of cardiac FPN and HAMP, possibly due to different local stimulatory and suppressive signals (e.g local inflammation, local ischemia), explain the reported lack of concordance between the degrees of cardiac iron overload and liver iron overload in a significant proportion of hemochromatosis and thalassemia major patients (42,43).

Iron deficiency is also detrimental to cardiac health. Indeed, systemic iron deficiency correlates with functional and molecular markers of disease severity in patients with chronic heart failure (CHF) (44,45),and also appears to contribute to the risk of death after an episode of acute heart failure (46). Given the high prevalence of iron deficiency in patients with CHF, ranging between 30-50% (44,47,48), the European Society of Cardiology recently recommended the assessment of iron deficiency as a comorbidity in CHF. Furthermore, several clinical trials have now established the benefits of intravenous iron supplementation

in CHF patients, with or without anaemia (49,50,51). The mechanisms underlying the anaemia-independent effects of iron deficiency and the benefits of intravenous iron in CHF patients are not fully understood. In light of the direct effect of cardiomyocyte iron deficiency on heart function, demonstrated in this and other studies, it would interesting to explore whether systemic iron deficiency in CHF patients is accompanied by cardiomyocyte iron deficiency, and whether correction of the later underlies the benefits of intravenous iron supplementation in non-anaemic patients.

Another open question is whether disruption of the cardiac HAMP/FPN axis contributes to the pathophysiology of heart disease. It has been shown, in the rat model of myocardial infarction (MI), that Hamp mRNA and HAMP protein are elevated in the ischemic myocardium during the acute phase (52). In humans, circulating HAMP was shown to be elevated in the serum within 4 hours of MI, although the tissue source of this hepcidin was not identified (53). In addition, decreased cardiac HAMP expression has been reported in a transgenic mouse model of dilated cardiomyopathy, where the phenotype was ameliorated following transgenic overexpression of cardiac hepcidin (54). Thus, further studies are warranted in humans to explore formally the role of the cardiac HAMP/FPN axis in the aetiology of heart disease.

Currently, there is considerable interest in targeting the HAMP/FPN axis for the treatment of iron overload and iron deficiency. Our studies suggest that such strategies may also impinge on cardiac iron homeostasis and function. Other than the heart, both FPN and hepcidin are also found in the brain, kidney and placenta (12,13,14,18,19,20,21). It would be important to establish whether our findings in the heart extend to these tissues.

MATERIALS & METHODS

Mice

All animal procedures were compliant with and approved under the UK Home Office Animals (Scientific Procedures) Act 1986. Both males and females were used in experiments, with the respective littermate control being of a matching sex.

The strategy for generating cardiac Hamp knockout mice is outlined in Appendix figure 4. Briefly, a targeting vector was designed to introduce a floxed *Hamp* allele into C57BL/6N mouse ES cells (JM8F6) with exons 2 and 3, which encode the majority of the peptide, flanked by LoxP sites and a line of floxed mice was generated by blastocyst injection of targeted ES cells, as previous described (15). Further breeding with a C57BL/6 Flp recombinase deleter mouse allowed removal of the Neomycin resistance cassette. Cardiac *Hamp* knockouts were then generated by by crossing $Hamp^{fl/fl}$ animals with mice transgenic for Cre recombinase, under the control of cardiomyocyte-specific Alpha Myosin Heavy Chain (*Myh6*) promoter (B6.FVB-Tg(*Myh6*-cre)2182Mds/J).The subsequent breeding strategy was designed to produce cardiac *Hamp* knockouts and homozygous floxed controls ($Hamp^{fl/fl}$;*Myh6.Cre*+ and $Hamp^{fl/fl}$ respectively) in the same litter.

The strategy for generating Cardiac *Slc40a1 C326Y* knock-in mice is outlined in Appendix figure 5, and further details are provided in the Appendix.

Cine MRI

Mice were anaesthetized with 2% isofluorane in O_2 and positioned supine in a purpose-built cradle. ECG electrodes were inserted into the forepaws, a respiration loop was taped across the chest and heart and respiration signals were monitored using a custom-built physiological motion gating device. The cradle was lowered into a vertical-bore, 11.7 T MR system with a 40-mm birdcage coil (Rapid Biomedical, Würzburg, Germany) and visualised using a Bruker console running Paravision 2.1.1. A stack of contiguous 1 mm thick true short-axis ECG and respiration-gated cine-FLASH images were acquired. The entire *in vivo* imaging protocol was performed in approximately 60 minutes. Image analysis was performed using ImageJ (NIH Image, Bethesda, MD). Left ventricular volumes and ejection fractions were calculated from the stack of cine images as described (15).

Dietary iron content

Unless otherwise stated, animals were provided with a standard rodent chow diet containing 200ppm iron. In iron manipulation experiments, mice were given an iron-deficient diet (2–5ppm iron; Teklad TD.99397; Harlan Laboratories), or an iron-loaded diet (5,000ppm iron;

Teklad TD.140464) or a matched control diet (200ppm iron; Teklad TD.08713) from weaning for 6 weeks.

Isolation of primary adult mouse cardiomyocytes and *in vitro* treatment

Adult primary cardiomyocytes were isolated from 8 week old C57BL/6 mice. Hearts were cannulated and mounted on a langendorff apparatus, then perfused using a liberase solution for 10 minutes. After filtration through a 400μm gauze, cells were cultured in MEM medium containing Hanks salts, L-glutamine and antibiotics. Within 2 hours of cardiomyocyte culture, supernatants were replaced with fresh medium containing 10% Fetal calf serum, with 0.5mmol/L ferric citrate (FAC) (F3388, Sigma Aldrich) or 100μmol/L desferroxamine (D9533, Sigma Aldrich) for 8 hours. The Furin inhibitor decanoyl-Arg-Val-Lys-Arg-chloromethylketone (CMK) (N1505, Bachem) was added at a concentration of 50μmol/L for the duration of DFO and FAC treatment.

Quantitative PCR

Total RNA extraction and cDNA synthesis were carried out as previously described (15). Gene expression was measured using Applied Biosystems Taqman gene expression assay probes for *Slc40a1, Hamp, TfR1*, *Myh7, Nppb, Ldha, Hk2, Eno* and house-keeping gene *β-Actin* (Life Technologies*, Carlsbad, CA*). The CT value for the gene of interest was first normalised by deducting CT value for *β-Actin* to obtain a delta CT value. Delta CT values of test samples were further normalised to the average of the delta CT values for control samples to obtain delta delta CT values. Relative gene expression levels were then calculated as $2^{-\text{delta deltaCT}}$.

Immunohistochemistry

Tissues were prepared as described previously (15) and stained with rabbit polyclonal anti-mouse HAMP antibody (ab30760, Abcam, RRID:AB_2115844) at 1/40 dilution, or rabbit polyclonal anti-mouse FPN antibody (MTP11-A, Alpha Diagnostics, RRID:AB_1619475) at 1/200 dilution. Results of control experiments confirming the specificity of the HAMP antibody are shown in Figure 1- Figure Supplement 5.

HAMP enzyme-linked immunosorbent assay (ELISA)

HAMP was measured in mouse sera and in cardiomyocyte supernatants using a HAMP ELISA kit (E91979Mu, USCN) according to the manufacturer's instructions. Results of control experiments confirming that *in vitro* treatments did not affect HAMP peptide detection by this ELISA kit are shown in Figure 1- Figure Supplement 6.

DAB-enhanced Perls stain

Formalin-fixed paraffin-embedded tissue sections were deparaffinised using Xylene, then rehydrated in ethanol. Slides were then stained for 1 hour with 1% potassium ferricyanide in 0.1mol/L HCl buffer. Endogenous peroxidase activity was quenched, then slides were stained with DAB chromogen substrate and counterstained with haematoxylin. They were visualised using a standard brightfield microscope.

Electron microscopy (EM)

Hearts were dissected and 0.5-1mm^3 slices were fixed by immersion for 2 hours in 2.5% glutaraldehyde in 0.1mol/L cacodylate buffer and prepared for electron microscopy by standard methods. Briefly, cells were post-fixed in osmium tetroxide (1% w/v in 0.1mol/L phosphate buffer), stained with uranyl acetate (2% w/v in distilled water), dehydrated through increasing concentrations of ethanol (70-100%) and acetone and embedded in TAAB resin (TAAB, Aldermaston, UK). Ultrathin sections (50-80nm) were prepared using a Reichert ultracut S microtome and mounted on 200 mesh nickel grids. Sections were lightly counterstained with lead citrate and uranyl acetate and examined with a Jeol transmission electron microscope (JEM-1010, JEOL, Peabody MA).

Fe55 efflux in primary adult cardiomyocytes

Adult cardiomyocytes were isolated from mice of the desired genotype at 9 weeks of age as described above. Cardiomyocytes were then cultured in 24-well plates at equal densities for 16 hours before the efflux experiment was performed as described (55). Briefly, after washing with 3 times PBS, cells were incubated for 30 minutes in 200µl uptake solution (98mmol/L NaCl, 2.0mmol/L KCl, 0.6mmol/L CaCl2, 1.0mmol/L MgCl2, 1.0mmol/L ascorbic acid, 10mmol/L HEPES [pH 6.0] with Tris base, 50µmol/L Fe55 (NEN, Boston, MA)), then washed 3 times with PBS and incubated for 30 minutes with efflux solution (98mmol/L NaCl,

2.0mmol/L KCl, 0.6mmol/L CaCl2, 1.0mmol/L MgCl2, 10mmol/L HEPES [pH 7.4] with Tris base, 300U/ml bovine ceruloplasmin (cp) (Sigma) and 40µg/ml human apotransferrin (tf) (Sigma)),in the absence or presence of 0.5µmol/L mouse HAMP peptide (Peptides International). The efflux medium was then removed, the cells washed 3 times in ice-cold PBS and disrupted by incubation in 100µl of 10% SDS solution for 10 minutes.The efflux solution and cell lysates were then transferred into scintillation vials for Fe55 counting. Where Furin inhibition was carried out, CMK was added to the culture medium at 50µmol/L 2 hours before the efflux experiment was carried out.

Iron quantitation

Ferritin concentration in serum and in liver lysates was determined using the ferritin ELISA kit (ICL, Inc. Portland). Serum iron levels were determined using the ABX-Pentra system (Horiba Medical, CA). Determination of total elemental iron in the heart was carried out by inductively coupled plasma mass spectrometry (ICP-MS) as described previously (15). Calibration was achieved using the process of standard additions, where spikes of 0ng/g, 0,5ng/g, 1ng/g, 10ng/g, 20ng/g and 100ng/g iron were added to replicates of a selected sample. An external iron standard (High Purity Standards ICP-MS-68-A solution) was diluted and measured to confirm the validity of the calibration. Rhodium was also spiked onto each blank, standard and sample as an internal standard at a concentration of 1ng/g. Concentrations from ICP-MS were normalised to starting tissue weight.

Isolation of cardiomyocyte and non-cardiomyocyte fractions for iron quantitation

Following cardiac perfusion, hearts were dissected into small pieces in ice-cold Hanks buffer, and subject to collagenase P digestion at 37C for 1 hour (11213857001, Roche Diagnostics). Following lysis of red blood cells, cell suspensions were passed through a 70µm sieve, before being labelled using cardiomyocyte isolation kit (130-100-825, Miltenyi Biotec). Separation of cardiomyocyte and non-cardiomyocyte fractions was carried out using MACS magnetic separation system according to the manufacturer's instructions. Cardiac fractions were lysed immediately for ICP-MS analysis.

Activity assays for aconitase I and electron transport chain (ETC) complexes

Approximately 10mg of frozen, crushed tissues were suspended in 200µl of ice-cold KME buffer (100mmol/L KCl, 50mmol/L Mops, 0.5mmol/L EGTA, pH 7.4), then homogenized by rupturing with a TissueRuptor (Qiagen) over ice. In a plastic cuvette, the cardiac lysate is mixed with assay buffer and slotted into a spectrophotometer. Details of assay buffers and of reaction procedure for each enzyme are detailed in the Appendix.

Statistics

Values are shown as mean± standard error of the mean (S.E.M). Comparison of iron indices, enzyme activities and parameters of cardiac function between groups was performed using Student's T test. P values <0.05 were deemed as indicating significant differences between groups. Where significant, exact p values for a figure panel are stated in the corresponding figure legend. No explicit power analysis was performed prior to the experiments to determine sample size, since we had no means to reliably estimate the size and variability of the effects of deleting hepcidin on parameters of cardiac function. For Cine MRI assessment of cardiac function, typically 5-11 animals of each genotype were used, with a matching number of littermate controls. For gene expression, iron quantitation and enzyme activity assays from mouse tissues, typically, 3-6 independent biological replicates and matching littermate controls were analysed. Since significant results were obtained from these set of experiments, no further animals were sacrificed. All "n" values reported refer to independent biological replicates.

ACKNOWLEDGEMENTS

We thank Yixing Wu, MRC Functional Genomic Unit, University of Oxford for his help with preparation of reagents for ETC complex assays.

We thank Prof Keith Dorrington, Dr Matthew Frise (Department of Physiology, Anatomy & Genetics, University of Oxford) and Dr Edward Littleton (University Hospitals Birmingham NHS Foundation Trust , Queen Elizabeth Hospital), for critical reading of the paper.

The authors declare no competing financial interests.

SLL was funded by the British Heart Foundation (Grant Number FS/12/63/29895) and the work was supported by Vifor Pharma and the Wellcome Trust Core Award Grant Number 090532/Z/09/Z.

REFERENCES

1. Rouault T, Klausner R. Regulation of iron metabolism in eukaryotes. *Current topics in cellular regulation*. 1997;35:1-19

2. Rouault TA. The role of iron regulatory proteins in mammalian iron homeostasis and disease. *Nature chemical biology*. 2006;2:406-414

3. Ganz T. Cellular iron: Ferroportin is the only way out. *Cell metabolism*. 2005;1:155-157

4. Donovan A, Lima CA, Pinkus JL, Pinkus GS, Zon LI, Robine S, Andrews NC. The iron exporter ferroportin/slc40a1 is essential for iron homeostasis. *Cell metabolism*. 2005;1:191-200

5. Nemeth E, Tuttle MS, Powelson J, Vaughn MB, Donovan A, Ward DM, Ganz T, Kaplan J. Hepcidin regulates cellular iron efflux by binding to ferroportin and inducing its internalization. *Science*. 2004;306:2090-2093

6. Qiao B, Sugianto P, Fung E, Del-Castillo-Rueda A, Moran-Jimenez MJ, Ganz T, Nemeth E. Hepcidin-induced endocytosis of ferroportin is dependent on ferroportin ubiquitination. *Cell metabolism*. 2012;15:918-924

7. Camaschella C. Understanding iron homeostasis through genetic analysis of hemochromatosis and related disorders. *Blood*. 2005;106:3710-3717

8. Musallam KM, Cappellini MD, Wood JC, Taher AT. Iron overload in non-transfusion-dependent thalassemia: a clinical perspective. *Blood Reviews*. 2012;26 Suppl 1:S16-19

9. De Falco L, Sanchez M, Silvestri L, Kannengiesser C, Muckenthaler MU, Iolascon A, Gouya L, Camaschella C, Beaumont C. Iron refractory iron deficiency anemia. *Haematologica*. 2013;98:845-853

525 **10.** Nemeth E, Ganz T. Anemia of inflammation. *Hematology/Oncology Clinics of North*
526 *America*. 2014;(4):671-81.
527 **11.** Merle U, Fein E, Gehrke S, Stremmel W, Kulaksiz H. The iron regulatory peptide
528 hepcidin is expressed in the heart and regulated by hypoxia and inflammation.
529 *Endocrinology*. 2007;148:2663–2668
530 **12.** McCarthy R, Kosman D. Glial cell ceruloplasmin and hepcidin differentially regulate iron
531 efflux from brain microvascular endothelial cells. PLoS One. 2014;9(2):89003.
532 **13.** Kulaksiz H, Theilig F, Bachmann S, Gehrke S, Rost D, Janetzko A, Cetin Y, Stremmel
533 W. The iron-regulatory peptide hormone hepcidin: expression and cellular localization in
534 the mammalian kidney. *Journal of Endocrinology*. 2005; 184:361–370.
535 **14.** Evans P, Cindrova-Davies T, Muttukrishna S, Burton G, Porter J, Jauniaux E. Hepcidin
536 and iron species distribution inside the first-trimester human gestational sac. *Molecular*
537 *Human Reproduction*. 2011;17 (4): 227-232.
538 **15.** Lakhal-Littleton S, Wolna M, Carr CA, Miller JJ, Christian HC, Ball V, Santos A, Diaz R,
539 Biggs D, Stillion R, Holdship P, Larner F, Tyler DJ, Clarke K, Davies B, Robbins PA.
540 Cardiac ferroportin regulates cellular iron homeostasis and is important for cardiac
541 function. *Proceedings of the National Academy of Sciences of the United States of*
542 *America*. 2015;112:3164-3169
543 **16.** Schimanski LM, Drakesmith H, Merryweather-Clarke AT, Viprakasit V, Edwards JP,
544 Sweetland E, Bastin JM, Cowley D, Chinthammitr Y, Robson KJ, Townsend AR. In vitro
545 functional analysis of human ferroportin (fpn) and hemochromatosis-associated fpn
546 mutations. *Blood*. 2005;105:4096-4102
547 **17.** Drakesmith H, Schimanski LM, Ormerod E, Merryweather-Clarke AT, Viprakasit V,
548 Edwards JP, Sweetland E, Bastin JM, Cowley D, Chinthammitr Y, Robson KJ,
549 Townsend AR. Resistance to hepcidin is conferred by hemochromatosis-associated
550 mutations of ferroportin. *Blood*. 2005;106:1092-1097
551 **18.** Rouault TA. Iron metabolism in the cns: Implications for neurodegenerative diseases.
552 *Nature reviews. Neuroscience*. 2013;14:551-564

553 **19.** Moos T, Rosengren Nielsen T. Ferroportin in the postnatal rat brain: Implications for
554 axonal transport and neuronal export of iron. *Seminars in pediatric neurology*.
555 2006;13:149-157
556 **20.** Bastin J, Drakesmith H, Rees M, Sargent I, Townsend A. Localisation of proteins of iron
557 metabolism in the human placenta and liver. *British journal of haematology*.
558 2006;134:532-543
559 **21.** Wolff N, Liu W, Fenton R, Lee W, Thevenod F, Smith C. Ferroportin 1 is expressed
560 basolaterally in rat kidney proximal tubule cells and iron excess increases its membrane
561 trafficking. *Journal of cellular and molecular medicine*. 2011;15:209-219.
562 **22.** Valore EV, Ganz T. Posttranslational Processing Of Hepcidin In Human Hepatocytes Is
563 Mediated By the Prohormone Convertase Furin. *Blood cells, molecules, and diseases.*
564 2008;40:132-138
565 **23.** Beaubien G, Schäfer MKH, Weihe E, Dong W, Chretien M, Sheidah NG, Day R. The
566 distinct gene expression of the pro-hormone convertases in the rat heart suggests
567 potential substrates. *Cell and tissue research*. 1995;279:539-549
568 **24.** Ichiki T, Boerrigter G, Huntley BK, Sangaralingham SJ, McKie PM, Harty GJ, Harders
569 GE, Burnett JC Jr. Differential expression of the pro-natriuretic peptide convertases
570 corin and furin in experimental heart failure and atrial fibrosis. *American Journal of*
571 *Physiology, Regulatory, Integrative and Comparative Physiology*. 2013;304:102-109
572 **25.** Ward DM, Kaplan J. Ferroportin-mediated iron transport: Expression and regulation.
573 *Biochimica et biophysica acta*. 2012;1823:1426-1433
574 **26.** Meyer J. Iron-sulfur protein folds, iron-sulfur chemistry, and evolution. *Journal of*
575 *biological inorganic chemistry : JBIC : a publication of the Society of Biological Inorganic*
576 *Chemistry*. 2008;13:157-170
577 **27.** Sono M, Roach MP, Coulter ED, Dawson JH. Heme-containing oxygenases. *Chemical*
578 *reviews*. 1996;96:2841-2888

28. Solomon EI, Decker A, Lehnert N. Non-heme iron enzymes: Contrasts to heme catalysis. *Proceedings of the National Academy of Sciences of the United States of America*. 2003;100:3589-3594

29. Belke DD, Larsen TS, Gibbs EM, Severson DL. Altered metabolism causes cardiac dysfunction in perfused hearts from diabetic (db/db) mice. *American journal of physiology. Endocrinology and metabolism*. 2000;279:E1104-1113

30. Kakinuma Y, Miyauchi T, Yuki K, Murakoshi N, Goto K, Yamaguchi I. Mitochondrial dysfunction of cardiomyocytes causing impairment of cellular energy metabolism induces apoptosis, and concomitant increase in cardiac endothelin-1 expression. *Journal of cardiovascular pharmacology*. 2000;36:S201-204

31. Ashrafian H, Frenneaux MP, Opie LH. Metabolic mechanisms in heart failure. *Circulation*. 2007;116:434-448

32. Dallman PR. Biochemical basis for the manifestations of iron deficiency. *Annual review of nutrition*. 1986;6:13-40

33. Dhur A, Galan P, Hercberg S. Effects of different degrees of iron deficiency on cytochrome p450 complex and pentose phosphate pathway dehydrogenases in the rat. *The Journal of nutrition*. 1989;119:40-47

34. Xu W, Barrientos T, Mao L, Rockman HA, Sauve AA, Andrews NC. Lethal cardiomyopathy in mice lacking transferrin receptor in the heart. *Cell reports*. 2015;13:533-545

35. Oexle H, Gnaiger E, Weiss G. Iron-dependent changes in cellular energy metabolism: Influence on citric acid cycle and oxidative phosphorylation. *Biochimica et biophysica acta*. 1999;1413:99-107

36. Schonekess BO, Allard MF, Henning SL, Wambolt RB, Lopaschuk GD. Contribution of glycogen and exogenous glucose to glucose metabolism during ischemia in the hypertrophied rat heart. *Circulation research*. 1997;81:540-549

37. Kato T, Niizuma S, Inuzuka Y, Kawashima T, Okuda J, Tamaki Y, Iwanaga Y, Narazaki M, Matsuda T, Soga T, Kita T, Kimura T, Shioi T. Analysis of metabolic remodeling in

compensated left ventricular hypertrophy and heart failure. *Circulation. Heart failure*. 2010;3:420-430

38. Tanne Z, Coleman R, Nahir M, Shomrat D, Finberg JP, Youdim MB. Ultrastructural and cytochemical changes in the heart of iron-deficient rats. *Biochemical pharmacology*. 1994;47:1759-1766

39. Walter PB, Knutson MD, Paler-Martinez A, Lee S, Xu Y, Viteri FE, Ames BN. Iron deficiency and iron excess damage mitochondria and mitochondrial DNA in rats. *Proceedings of the National Academy of Sciences of the United States of America*. 2002;99:2264-2269

40. Silvestri L, Pagani A, Camaschella C. Furin-mediated release of soluble hemojuvelin: a new link between hypoxia and iron homeostasis. *Blood.* 2008;111:924-931

41. Gulati V, Harikrishnan P, Palaniswamy C, Aronow WS, Jain D, Frishman WH. Cardiac involvement in hemochromatosis. *Cardiology in review*. 2014;22:56-68

42. Anderson LJ, Holden S, Davis B, Prescott E, Charrier CC, Bunce NH, Firmin DN, Wonke B, Porter J, Walker JM, Pennell DJ. Cardiovascular t2-star (t2*) magnetic resonance for the early diagnosis of myocardial iron overload. *European heart journal*. 2001;22:2171-2179

43. Noetzli LJ, Carson SM, Nord AS, Coates TD, Wood JC. Longitudinal analysis of heart and liver iron in thalassemia major. *Blood*. 2008;112:2973-2978

44. Klip IT, Comin-Colet J, Voors AA, Ponikowski P, Enjuanes C, Banasiak W, Lok DJ, Rosentryt P, Torrens A, Polonski L, van Veldhuisen DJ, van der Meer P, Jankowska EA. Iron deficiency in chronic heart failure: An international pooled analysis. *American heart journal*. 2013;165:575-582 e573

45. Comin-Colet J, Enjuanes C, Gonzalez G, Torrens A, Cladellas M, Merono O, Ribas N, Ruiz S, Gomez M, Verdu JM, Bruguera J. Iron deficiency is a key determinant of health-related quality of life in patients with chronic heart failure regardless of anaemia status. *European journal of heart failure*. 2013;15:1164-1172

634 **46.** Jankowska EA, Kasztura M, Sokolski M, Bronisz M, Nawrocka S, Oleskowska-Florek W,
635 Zymlinski R, Biegus J, Siwolowski P, Banasiak W, Anker SD, Filippatos G, Cleland JG,
636 Ponikowski P. Iron deficiency defined as depleted iron stores accompanied by unmet
637 cellular iron requirements identifies patients at the highest risk of death after an episode
638 of acute heart failure. *European heart journal*. 2014;35:2468-2476
639 **47.** Nanas JN, Matsouka C, Karageorgopoulos D, Leonti A, Tsolakis E, Drakos SG,
640 Tsagalou EP, Maroulidis GD, Alexopoulos GP, Kanakakis JE, Anastasiou-Nana MI.
641 Etiology of anemia in patients with advanced heart failure. *Journal of the American*
642 *College of Cardiology*. 2006;48:2485-2489
643 **48.** Ezekowitz JA, McAlister FA, Armstrong PW. Anemia is common in heart failure and is
644 associated with poor outcomes: Insights from a cohort of 12 065 patients with new-onset
645 heart failure. *Circulation*. 2003;107:223-225
646 **49.** Ponikowski P, van Veldhuisen DJ, Comin-Colet J, Ertl G, Komajda M, Mareev V,
647 McDonagh T, Parkhomenko A, Tavazzi L, Levesque V, Mori C, Roubert B, Filippatos G,
648 Ruschitzka F, Anker SD, Investigators C-H. Beneficial effects of long-term intravenous
649 iron therapy with ferric carboxymaltose in patients with symptomatic heart failure and
650 iron deficiencydagger. *European heart journal*. 2015;36:657-668
651 **50.** Anker SD, Comin Colet J, Filippatos G, Willenheimer R, Dickstein K, Drexler H, Luscher
652 TF, Bart B, Banasiak W, Niegowska J, Kirwan BA, Mori C, von Eisenhart Rothe B,
653 Pocock SJ, Poole-Wilson PA, Ponikowski P, Investigators F-HT. Ferric carboxymaltose
654 in patients with heart failure and iron deficiency. *The New England journal of medicine*.
655 2009;361:2436-2448
656 **51.** Avni T, Leibovici L, Gafter-Gvili A. Iron supplementation for the treatment of chronic
657 heart failure and iron deficiency: Systematic review and meta-analysis. *European journal*
658 *of heart failure*. 2012;14:423-429
659 **52.** Simonis G, Mueller K, Schwarz P, Wiedemann S, Adler G, Strasser RH, Kulaksiz H. The
660 iron-regulatory peptide hepcidin is upregulated in the ischemic and in the remote
661 myocardium after myocardial infarction. *Peptides*. 2010;31:1786-1790

662 **53.** Suzuki H, Toba K, Kato K, Ozawa T, Tomosugi N, Higuchi M, Kusuyama T, Iso Y,
663 Kobayashi N, Yokoyama S, Fukuda N, Saitoh H, Akazawa K, Aizawa Y. Serum
664 hepcidin-20 is elevated during the acute phase of myocardial infarction. *The Tohoku*
665 *journal of experimental medicine*. 2009;218:93-98
666 **54.** Zhang L, Lu D, Zhang W, Quan X, Dong W, Xu Y, Zhang L. Cardioprotection by hepc1
667 in ctnt(r141w) transgenic mice. *Transgenic research*. 2012;21:867-878
668 **55.** McKie AT, Marciani P, Rolfs A, Brennan K, Wehr K, Barrow D, Miret S, Bomford A,
669 Peters TJ, Farzaneh F, Hediger MA, Hentze MW, Simpson RJ. A novel duodenal iron-
670 regulated transporter, IREG1, implicated in the basolateral transfer of iron to the
671 circulation. *Molecular Cell.* 2000;5:299-309
672 **56.** Liu P, Jenkins NA, Copeland NG. A highly efficient recombineering-based method for
673 generating conditional knockout mutations. *Genome research.* 2003;13:476-484
674 **57.** Brooks KJ, Hargreaves IP, Bates TE. Nitric-oxide-induced inhibition of mitochondrial
675 complexes following aglycaemic hypoxia in neonatal cortical rat brain slices.
676 *Developmental Neuroscience*. 2000;22:359-65.
677

678 **APPENDIX**

679 **Generation of *Slc40a1* C326Y$^{fl/fl}$ mice.** A C57BL/6J mouse genomic BAC clone (RP23-183-
680 P22) encompassing the *Slc40a1* gene was used for the generation of the targeting vector. A
681 12 kb region of the RP23-183-P22 encompassing exons 6-8 and surrounding intronic
682 regions was subcloned by gap-repair into a plasmid containing a diphtheria toxin A chain
683 negative selection cassette. The required C326Y point mutation was introduced into this
684 subclone by site directed mutagenesis. In parallel, a loxP flanked neomycin/kanamycin
685 selection cassette (from PL452 [56]) was inserted into the BAC within *Slc40a1* intron 6 by
686 recombineering and an approximately 5 kb ApaI/PmeI fragment encompassing this insertion
687 together with exons 6 and 7 and flanking introns was subcloned into pBluescript. This
688 plasmid was treated with Cre recombinase (NEB) in vitro to remove the selection cassette,

689 resulting in a plasmid containing a single loxP and an additional SpeI site within *Slc40a1*
690 intron 6. This loxP interrupted sequence was shuttled into the genomic subclone by
691 exchanging an internal NcoI fragment. A portion of *Slc40a1* cDNA corresponding to the
692 coding region encoded on exons 7 and 8, including the 3' untranslated region was amplified
693 by RT-PCR from cDNA prepared from embryonic mouse heart and inserted into a piece of
694 synthetic DNA (Gene Art) corresponding to intronic and intergenic sequence lying
695 immediately upstream of exon 7 and downstream of exon 8, respectively. This minigene
696 assembly was cloned upstream of an FRT-PGK-Neomycin-FRT-loxP selection cassette
697 (from P451[56]) and the two pieces together were inserted into the modified genomic subclone
698 above via a unique SacII site, completing the final targeting vector. The completed targeting
699 vector was linearised with AatII and electroporated into C57BL/6N JM8F6 embryonic stem
700 cells. Following selection in 210µg/ml G418, recombinant clones were screened by PCR to
701 detect homologous recombination over the 3' arm. A forward primer (5'-
702 CAATAGCAGGCATGCTGGGGATG-3') binding within the polyadenylation of the selection
703 cassette was used together with a reverse primer (5'- GGCATCTGCTGTCTGTGAAA- 3')
704 binding downstream of the 3' homology arm to amplify a 6.6 kb fragment from correctly
705 recombined clones. Positive clones were examined for correct recombination at the 5' end
706 by long range PCR using a forward primer (5'- TGTACCATGGATGGGTCCTT-3') binding
707 upstream of the 5' homology arm and a reverse primer (5'-
708 TACCGGTGGATGTGGAATGTG- 3') binding within the PGK promoter driving the neomycin
709 selection. Correctly targeted clones yielded a 9.7 kb amplicon. Incorporation of the 5' loxP
710 site, was verified by digestion of this 5' amplicon with SpeI which yielded a 7kb and 2.7 kb
711 cleavage products in correctly targeted clones. Both 5' and 3' screening amplicons were
712 analysed by Sanger sequencing to confirm the junction sequence over the extremities of the
713 homology arms using sequencing primers 5'-AAAGCCCAGGGGTATCTCTC-3' and 5'-
714 CTCAGCTTGGCTATGTGGTG-3' for the 5' and 3' amplicons respectively. The presence of
715 the 5' loxP site within the 5' amplicon was confirmed by Sanger sequencing using
716 sequencing primer 5'- CATGAAGCAGTGGGCATAGA-3' and the presence of the C326Y

717 mutation was confirmed within the 3' amplicon using sequencing primer 5'-
718 CACACACACACATATATACATGCAA-3'. Southern blotting using a probe against neomycin
719 was used to confirm that only a single integration event had occurred. Correctly recombined
720 ES cells were injected into albino C57BL/6J blastocysts and the resulting chimeras were
721 mated with albino C57BL/6J females. Successful germline transmission yielded black pups
722 and F1 mice harboring the conditional C326Y knock-in allele were identified using the above
723 screening PCR. F1 heterozygous male mice were bred with C57BL/6J Flp recombinase
724 deleter mice (Tg(ACTB-Flpe)9205Dym (Jax stock 005703)) and offspring were screened for
725 the deletion of the selection cassette using a forward primer (5'-
726 GATATCATCATCGCCCTTTGG- 3') binding within the 3' untranslated region of the exon 7-8
727 minigene and a reverse primer (5'- TTGCATGTATATATGTGTGTGTGTG-3') binding
728 immediately downstream of the cassette. A 1.4 kb amplicon was obtained from the Flp
729 deleted conditional C326Y knock-in allele. Heterozygous mice without the selection cassette
730 were then backcrossed with C57BL/6J to remove the Flp transgene prior to onward
731 breeding.

732 **Aconitase and ETC activities**

733 **Total aconitase I activity assay:** Total aconitase I activity was measured as the rate of
734 isomerization of cis-aconitic to isocitrate at 240nm and 37°C using a spectrophotometer. The
735 assay buffer consisted of 50mmol/L Tris HCl pH 7.5. The reaction was carried out in a quartz
736 cuvette containing 1ml assay buffer supplemented with 10µl 20nmol/L cis-aconitic acid
737 (Sigma) and 25µl of protein lysate and read for 2 minutes at 240nm against a black
738 containing ddH_2O. The activity of aconitase was determined by dividing the gradient of the
739 absorbance over the extinction coefficient (3600) and expressed in nmol/min/mg tissue.

740 **Complex I activity assay:** Mitochondrial complex I activity was measured as the rate of
741 NADH oxidation at 340nm and 30°C using a spectrophotometer. The assay buffer contained
742 the following: 25Mmol/L potassium phosphate pH 7.2, 5mmol/L $MgCl_2$ (Sigma), 0.13mmol/L
743 NADH (MP Biomedicals, LLP), 65µM coenzyme Q_1 (Sigma), 250mg fatty acid free BSA

744 (Sigma), 200µg antimycin A (Santa Cruz). The reaction was carried out in 1ml assay buffer
745 supplemented with 20µl of protein lysate and read for 1 minute at 340nm against a blank
746 containing ddH_2O. As a negative control, 20µl of 10mmol/Lrotenone (Sigma) was added to a
747 new reaction and the inhibited rate measured for 1 minute. The activity of complex I was
748 determined by dividing the gradient of the absorbance over the extinction coefficient (6810)
749 and expressed in nmol/min/mg tissue.

750 **Complex II activity assay:** Mitochondrial complex II activity was measured as the rate of
751 succinate-dependent reduction of dichlorophenolindophenol (DCIP) at 600nm and 30°C
752 using a spectrophotometer. The assay buffer contained the following: 25mol/L potassium
753 phosphate pH 7.2, 5mmol/L $MgCl_2$, and 2mmol/L sodium succinate dibasic hexahydrate
754 (Sigma). The reaction was carried out in 985µl of assay buffer supplemented by 10µl of
755 buffer containing 2µg antimycin, 2µg rotenone, 50µmol/L DCIP (Sigma) followed by addition
756 of 65µmol/L CoQ_1 and 20µl protein lysate and read for 2 minutes at 600nm against a blank
757 containing ddH_2O. As a negative control, 20µl of 10mmol/L sodium malonate (Sigma) was
758 added to a new reaction and the inhibited rate measured for 2 minutes. The activity of
759 complex II was determined by dividing the gradient of the absorbance over the extinction
760 coefficient (21000) and expressed in nmol/min/mg tissue.

761 **Complex III activity assay:** Mitochondrial complex III activity was measured as the rate of
762 reduction of cytochrome c^{3+} at 550nm at 30°C using reduced ubiquinol as an electron
763 acceptor using a spectrophotometer. To prepare ubiquinol, 10mg of decylubiquinone
764 (Sigma) was dissolved in 312.5µl absolute ethanol to give a final concentration of
765 100mmol/L. An aliquot of 100µl decylubiquinone working solution was further diluted in 900µl
766 ethanol and acidified to pH 2 with a 6mol/L HCl solution. The ubiquinone was then reduced
767 with a pinch of sodium borohydrate (Sigma) and 1ml of ddH_2O was added to stop the
768 reaction. Excess sodium borohydrate was allowed to settle and the sample centrifuged
769 briefly to separate the sodium borohydrate precipitate from the reduced ubiquinol. Using a
770 pH indicator paper, the pH of the ubiquinol was verified to be at pH 2 before using in the

activity assay. The reaction was carried in 1ml of assay buffer (50mM potassium phosphate pH 7.2, 3mmol/L sodium azide (Sigma), 1.5µmol/L rotenone, and 50µmol/L cytochrome c from bovine heart (Sigma)), supplemented with 5µl reduced ubiquinol and 20µl protein lysate and read for 1 minute at 550nm against a blank containing ddH_2O. As a negative control, 10µl of 20mmol/L antimycin A was added to a new reaction and the inhibited rate measured for 1 minute. As further negative control, a reaction containing protein only or reduced ubiquinol only was also measured for 1 minute. The activity of complex III was determined by dividing the gradient of the absorbance over the extinction coefficient (19100) and expressed in nmol/min/mg tissue.

Complex IV activity assay: Mitochondrial complex IV activity was measured as the rate of oxidation of cytochrome c^{2+} at 550nm at 30°C using a spectrophotometer. To prepare the reduced cytochrome c^{2+}, a dialysis tubing (Viking 7000/1) of appropriate length was hydrated for 30 minutes in 1L ddH_2O supplemented with 20g sodium carbonate and 0.372g EDTA at 80°C. A solution of 100mg of cytochrome c from bovine heart and 10mg sodium ascorbate dissolved in 10ml potassium phosphate (0.1mol/L, pH 7.0) was added to the tubing and dialysed against 1L of 0.1mol/L potassium phosphate buffer for 24h at 4°C. The phosphate buffer was exchanged 3 times, every 8h. The redox state of the synthesized reduced cytochrome c was verified by measuring the absorbance spectra between wavelengths of 500 and 600nm, in the presence or absence of 100µmol/L potassium ferricyanide (Sigma) and compared against the oxidized cytochrome c. The reaction was carried out in 1ml assay buffer (10mmol/L potassium phosphate pH 7.0 and 0.50µmol/L reduced cytochrome c) supplemented with 5µl protein lysate and read for 3 minutes at 550nm against a blank of assay buffer supplemented by 100µmol/L potassium ferricyanide. As a negative control, 10µl of 10mmol/L sodium azide was added to a new reaction and the inhibited rate measure for 3 minutes. The first-order rate constant (k) was calculated as previously described[57]. Briefly, the natural logarithm was taken for the absorbances at 4 time points t=0, 60, 120, 180 seconds and the difference for each pair of time points determined (t(60)-t(0), t(120)-t(60),

t(180)-t(120)). The average of these differences were taken to be k and the activity expressed in nmol/min/mg tissue.

LIST OF FIGURE SUPPLEMENTS

Figure 1- Figure Supplement 1

Figure 1- Figure Supplement 2

Figure 1- Figure Supplement 3

Figure 1- Figure Supplement 4

Figure 1- Figure Supplement 5

Figure 1- Figure Supplement 6

Figure 3- Figure Supplement 1

Figure 3- Figure Supplement 2

LIST OF SUPPLEMENTARY FILES

Appendix figure 1

Appendix figure 2

Appendix figure 3

Appendix figure 4

Appendix figure 5

Appendix figure 6

LIST OF SOURCE DATA FILES

Figure 2- source data 1

Figure 3- source data 1

Figure 4- source data 1

	Hamp$^{fl/fl}$	*Hamp*$^{fl/fl}$*;Myh6.Cre+*
liver total elemental iron (ng/mg tissue)	96.3±12.2	88.7±19.2
liver ferritin (µg/mg total protein)	0.65±0.04	0.64±0.05
serum iron (µmol/L)	28.60±7.20	31.50±8.40
serum ferritin (mg/L)	1.81±0.04	1.88±0.29
hemoglobin (g/L)	122.7±11.5	116.0±11.9
serum hepcidin (µg/L)	23.5±7.6	23.9±10.40

Table 1: Indices of systemic iron in 6 month old *Hamp*$^{fl/fl}$ and *Hamp*$^{fl/fl}$*;Myh6.Cre+* mice. n=6 per group. All values are shown as mean±SEM.

	3 months		6 months		9 months	
	Hamp $^{fl/fl}$	*Hamp* $^{fl/fl}$; *Myh6.Cre+*	*Hamp* $^{fl/fl}$	*Hamp* $^{fl/fl}$; *Myh6.Cre+*	*Hamp* $^{fl/fl}$	*Hamp* $^{fl/fl}$; *Myh6.Cre+*
Average mass (mg)	70.51±7.47	70.38±5.33	72.59±5.38	82.54±11.32	78.30±4.92	83.07±5.44
RVED lumen (µl)	31.37±2.55	26.81±2.30	33.12±3.19	30.63±2.35	38.39±3.88	39.95±3.00
RVES lumen (µl)	7.43±0.79	5.23±0.67	8.70±1.22	8.34±1.06	13.36±2.21	15.51±2.47
RVEF (%)	76.42±1.32	79.88±2.80	73.66±2.50	73.42±2.22	65.20±4.36	61.95±3.53
Stroke volume (µl)	25.47±1.99	22.73±2.11	25.70±2.70	23.76±1.85	29.79±2.30	29.84±1.59
Cardiac output (ml/min)	10.34±1.06	9.62±0.90	10.72±1.07	10.53±1.05	11.46±1.15	11.99±1.38
Heart Rate (bpm)	404.07±18.69	426.90±17.94	419.64±19.05	436.14±14.30	384.84±28.55	400.97±41.20
Heart/body weight ratio x1000	2.80±0.18	3.09±0.26	2.51±0.23	2.98±0.37	2.36±0.28	2.88±0.27

Table 2: Non-LV parameters of cardiac function are not altered between *Hamp*$^{fl/fl}$ and *Hamp*$^{fl/fl}$*;;Myh6.Cre+* mice. Cine MRI measurements of cardiac function in *Hamp*$^{fl/fl}$*;Myh6.Cre+* mice and *Hamp*$^{fl/fl}$ controls at 3 months (n=8 per group), 6 months (n=11 per group) and 9 months (n=5 per group) of age. Values are shown as mean±SEM.

	Slc40a1 C326Y$^{fl/fl}$	*Slc40a1* C326Y $^{fl/fl}$; *Myh6.Cre+*
liver total elemental iron (ng/mg tissue)	92.77±21.30	84.00±26.00
liver ferritin (µg/mg total protein)	0.87±0.06	0.92±0.05
serum iron (µmol/L)	27.30±5.20	29.60±7.20
serum ferritin (mg/L)	2.10±0.04	2.20±0.15
hemoglobin (g/L)	125.70±8.80	126.00±12.30
serum hepcidin (µg/L)	25.90±11.60	27.50±8.40

Table 3: Characterisation of *Slc40a1* C326Y$^{fl/fl}$*;Myh6.Cre+* mice. Indices of iron status in *Slc40a1* C326Y$^{fl/fl}$ and *Slc40a1* C326Y$^{fl/fl}$*;Myh6.Cre+* mice at 6 months of age (n=4 per group). Values are shown as mean±SEM.

	Hamp$^{fl/fl}$		*Hamp* $^{fl/fl}$*;Myh6.Cre+*	
	untreated	treated with I.V iron	untreated	treated with I.V iron
cardiac total elemental iron (ng/mg tissue)	82.2±16.9	331.3±21.5*	74.9±7	399.8±68.5†
liver total elemental iron (ng/mg tissue)	100.4±11	2527.6±27.63*	96.3±14	2258.2±239.9†
serum iron (µmol/L)	30.09±6.37	74.48±17.96*	31.5±6.9	80.12±24.9†
serum hepcidin (µg/L)	27.41±6.7	237.3±16.7*	28.9±9.4	209.8±38.8†

Table 4: Effect of intravenous iron treatment on iron indices.

Total cardiac and liver elemental iron, serum iron and circulating HAMP in 6-month old untreated and I.V iron-treated *Hamp*$^{fl/fl}$*;Myh6.Cre+* mice and *Hamp*$^{fl/fl}$ littermate controls. Treated mice were injected with 0.5mg iron fortnighly from the age of 3 months. Tissues and serum were harvested 12 hours after the final injection. n=5 per group. *p<0.05 relative to

841 untreated *Hamp*$^{fl/fl}$ mice. †p<0.05 relative to untreated *Hamp*$^{fl/fl}$*;Myh6.Cre*+ . Values are
842 shown as mean±SEM.
843
844 **FIGURE LEGENDS**
845 **Figure 1: Hepcidin expression and regulation in the heart**. (**A)** Relative *Hamp* mRNA
846 expression in heart and liver of adult C57BL/6 mice, under control conditions and after
847 provision of low or high iron diets. *p=0.047, 0.001 respectively relative to control hearts,
848 †p=0.006, 0.019 respectively relative to control livers. (**B)** Corresponding
849 immunohistochemical staining for HAMP in heart and liver. **(C)** Relative *Hamp* mRNA
850 expression in primary adult mouse cardiomyocytes cultured under control conditions or in
851 presence of FAC or DFO. *p=0.023, 0.001 and 0.014 respectively relative to control.
852 †p=0.024, 0.037, 0.016 and 0.037 respectively relative to control at the same timepoint. **(D)**
853 Corresponding HAMP protein levels in supernatants of primary cardiomyocytes. DFO
854 treatment was carried alone (DFO) or presence of Furin inhibitor (DFO+CMK). *p=0.002,
855 0.020, 0.028, 0.014, 0.015 respectively relative to control at the same timepoint**. (E)** Relative
856 *Hamp* expression in heart and liver of 3 month old *Hamp*$^{fl/fl}$ and *Hamp*$^{fl/fl}$*;Myh6.Cre*+ mice.
857 *p=0.018 relative to cardiac *Hamp* in *Hamp*$^{fl/fl}$ controls. **(F)** Corresponding
858 immunohistochemical staining for HAMP in heart and liver. All values are plotted as
859 mean±SEM. Scale bar=20μm. n=3 per group unless otherwise stated. Figure 1-Figure
860 Supplement 1- Cardiac and liver iron content following dietary iron manipulation. Figure
861 Supplement 2- Furin regulation by iron. Figure 1-Figure Supplement 3- Relative Hamp
862 mRNA expression in cardiomyocytes following treatment with Furin inhibitor. Figure 1-Figure
863 Supplement 4- HAMP in supernatants of cardiomyocytes from *Hamp*$^{fl/fl}$;;*Myh6.Cre*+ mice.
864 Figure 1-Figure Supplement 5- Confirmation of HAMP antibody specificity. Figure 1- Figure
865 Supplement 6- HAMP detection by ELISA unaffected by FAC and DFO.
866

Figure 2: Fatal cardiac abnormalities in *Hamp*$^{fl/fl}$;*Myh6.Cre*+ mice. (A) Cumulative survival of *Hamp*$^{fl/fl}$;*Myh6.Cre*+ mice (n=50) and *Hamp*$^{fl/fl}$ littermate controls (n=47) over 52 weeks. **(B)** Representative H&E longitudinal heart sections from a 6 month old *Hamp*$^{fl/fl}$;*Myh6.Cre*+ mouse and *Hamp*$^{fl/fl}$ littermate control. **(C)** Representative WGA cardiac staining from a 6 month old *Hamp*$^{fl/fl}$;*Myh6.Cre*+ mouse and *Hamp*$^{fl/fl}$ littermate control. **(D)** Quantitation of cardiomyocyte size based on WGA staining in 6 month old *Hamp*$^{fl/fl}$;*Myh6.Cre*+ mice and *Hamp*$^{fl/fl}$ littermate controls. *p=0.001 relative to *Hamp*$^{fl/fl}$ littermate controls. **(E)** Relative expression of the hypertrophic gene markers *Myh7* and *Nppb* in hearts of 6 month old *Hamp*$^{fl/fl}$;*Myh6.Cre*+ mice and *Hamp*$^{fl/fl}$ littermate controls. *p=0.001, 0.047 for the respective gene relative to *Hamp*$^{fl/fl}$ littermate controls. **(F)** Representative cardiac in-situ TUNEL staining from a 6 month old *Hamp*$^{fl/fl}$;*Myh6.Cre*+ mouse and *Hamp*$^{fl/fl}$ littermate control. **(G)** Quantitation of percentage of apoptotic cardiomyocytes based on in-situ TUNEL staining in 6 month old *Hamp*$^{fl/fl}$;*Myh6.Cre*+ mice and *Hamp*$^{fl/fl}$ littermate controls *p=0.001 relative to *Hamp*$^{fl/fl}$ littermate controls. **(H)** Representative midventricular Cine MR images of hearts from *Hamp*$^{fl/fl}$;*Myh6.Cre*+ mice and *Hamp*$^{fl/fl}$ controls at 3 , 6 and 9 months of age. **(I-K)** Cine MRI measurements of LV lumen, at end-systole (LVES), end-diastole (LVED), and of ejection fraction (LVEF) in *Hamp*$^{fl/fl}$;*Myh6.Cre*+ mice and *Hamp*$^{fl/fl}$ littermate controls at 3 months (n=8 per group), 6 months (n=11 per group, *p=0.043 for LVES, 0.047 for LVED and 0.020 for LVEF) and 9 months (n=5 per group, *p=0.044 for LVES, 0.042 for LVED and 0.034 for LVEF). p values are relative to *Hamp*$^{fl/fl}$ controls of the respective age. All Values are plotted as mean±SEM. n=3 per group unless otherwise stated. Scale bar= 50μm.

Figure 3: The role of cardiomyocyte FPN. (A-B) Immunohistochemical staining for FPN in the hearts of 3 month old *Hamp*$^{fl/fl}$;*Myh6.Cre*+, *Slc40a1 C326Y*$^{fl/fl}$;*Myh6.Cre*+ mice and respective controls. **(C)** Cumulative survival of *Slc40a1 C326Y*$^{fl/fl}$;*Myh6.Cre*+ mice (n=36)

and *Slc40a1 C326Y*$^{fl/fl}$ littermate controls (n=31) over 52 weeks. **(D)** Representative H&E-stained longitudinal heart sections from a 6 month old *Slc40a1 C326Y*$^{fl/fl}$;*Myh6.Cre*+ mouse and a *Slc40a1 C326Y*$^{fl/fl}$ control. **(E)** Representative WGA cardiac staining from a 6 month old *Slc40a1 C326Y*$^{fl/fl}$;*Myh6.Cre*+ mouse and *Slc40a1 C326Y*$^{fl/fl}$ control. **(F)** Quantitation of cardiomyocyte size based on WGA staining. n=3 per group. *p=0.001 relative to *Slc40a1 C326Y*$^{fl/fl}$ controls. **(G)** Relative expression of *Myh7* and *Nppb* in hearts of 6 month old *Slc40a1 C326Y*$^{fl/fl}$;*Myh6.Cre*+ mice and *Slc40a1 C326Y*$^{fl/fl}$ controls. n=3 per group. *p=0.032, 0.044 for the respective gene relative to *Slc40a1 C326Y*$^{fl/fl}$ controls. (**H)** Representative cardiac TUNEL staining from a 6 month old *Slc40a1 C326Y*$^{fl/fl}$;*Myh6.Cre*+ mouse and *Slc40a1 C326Y*$^{fl/fl}$ control. **(I)** Quantitation of percentage of apoptotic cardiomyocytes based on TUNEL staining, n=3 per group. *p=0.0003 relative to *Slc40a1 C326Y*$^{fl/fl}$ controls. **(J-L)** Cine MRI measurements of LVES, LVED and LVEF in *Slc40a1 C326Y*$^{fl/fl}$;*Myh6.Cre*+ mice and *Slc40a1 C326Y*$^{fl/fl}$ controls at 3 months (n=6 per group), 6 months (n=6 per group, *p=0.003 for LVES, 0.043 for LVED and 0.001 for LVEF) and 9 months (n=5 per group, *p= 0.033 for LVES, 0.047 for LVED and 0.023 for LVEF). P values are relative to *Slc40a1 C326Y*$^{fl/fl}$ controls of the same age. **(M)** Percentage Fe55 efflux in cardiomyocytes from *Hamp*$^{fl/fl}$;*Myh6.Cre*+ mice, *Slc40a1 C326Y*$^{fl/fl}$;*Myh6.Cre*+ mice and respective controls, in presence or absence of HAMP peptide. *p=0.018, 0.006 and 0.007 respectively **(N)** Elemental iron levels in cardiomyocyte fractions (CF) from the hearts of *Hamp*$^{fl/fl}$;*Myh6.Cre*+ mice, *Slc40a1 C326Y*$^{fl/fl}$;*Myh6.Cre*+ mice and their respective controls. n=4 per group. *p=0.032, 0.044, 0.047 and 0.031 respectively. **(O-P)** Relative *TfR1* (*p=0.038, 0.001) and *Fpn* (*p=0.039, 0.047) expression in hearts of 3 month old *Hamp*$^{fl/fl}$;*Myh6.Cre*+ mice, *Slc40a1 C326Y*$^{fl/fl}$;*Myh6.Cre*+ mice and their respective controls. All values are plotted as mean±SEM. Scale bar=50μm. Figure supplement 1- Characterisation of *Slc40a1 C326Y*$^{fl/fl}$;*Myh6.Cre*+ mice. Figure supplement 2- Total cardiac iron levels.

Figure 4: **The role of cardiomyocyte iron deficiency and metabolic derangement in cardiac dysfunction. (A-C)** Cine MRI measurements of LV lumen, at end-systole (LVES, *p=0.048), end-diastole (LVED, *p=0.031), and of ejection fraction (LVEF, *p=0.004) in 6-month old untreated (-iron) and I.V iron-treated (+iron) *Hamp*$^{fl/fl}$;*Myh6.Cre*+ mice and *Hamp*$^{fl/fl}$ littermate controls. n=5 per group. **(D-E)** Relative *TfR1* (*p=0.001) and *Fpn* (*p=0.002) expression in hearts of 6-month old untreated (-iron) and I.V iron-treated (+iron) *Hamp*$^{fl/fl}$;*Myh6.Cre*+ mice and *Hamp*$^{fl/fl}$ littermate controls. n=4 per group. **(F-H)** Enzymatic activities of Aconitase I (*p=0.035, 0.041) , Complex I (*p=0.004, 0.030) and Complex IV (*p=0.003, 0.026) in untreated (-iron) 3-month and 6-month old and in I.V iron-treated (+iron) 6-month old *Hamp*$^{fl/fl}$;*Myh6.Cre*+ mice and *Hamp*$^{fl/fl}$ littermate controls. n=4 per group. **(I)** Representative EM micrographs of hearts from untreated (-iron) 3-month and 6-month old and I.V iron-treated (+iron) 6-month old *Hamp*$^{fl/fl}$;*Myh6.Cre*+ mice and *Hamp*$^{fl/fl}$ littermate controls. Scale bar=2μm. **(J-L)** Relative *Hk2* (*p=0.010, 0.002), *Eno* (*p=0.014, 0.021) and *Ldha* (*p=0.003, 0.001) expression levels in hearts of untreated (-iron) 3-month and 6-month old and in I.V iron-treated (+iron) 6-month old *Hamp*$^{fl/fl}$;*Myh6.Cre*+ mice and *Hamp*$^{fl/fl}$ littermate controls. n=4 per group. NS=not significant. All values are plotted as mean±SEM

Figure 5: Interplay between systemic and cardiac iron HAMP/FPN axes. Cardiomyocyte iron content is determined by both systemic iron availability, which is regulated by liver HAMP, and by the cardiac HAMP/FPN axis, which regulates cardiomyocyte iron efflux. In the wild type heart, cardiac HAMP regulates the levels of cardiac FPN and iron release from cardiomyocytes. In this study, we have demonstrated that loss of cardiac HAMP (cardiac Hamp KO) or loss of cardiac HAMP responsiveness (cardiac Slc40a1 C326Y KI) result in cardiomyocyte iron deficiency due to increased cardiomyocyte FPN and iron release. Previously, we also demonstrated that loss of cardiomyocyte FPN caused cardiomyocyte iron overload. In these two sets of conditions, cardiomyocyte iron deficiency and cardiomyocyte iron overload cause cardiac dysfunction. We have also shown that upregulation of cardiac FPN occurs as a result of loss of either systemic HAMP or systemic

HAMP responsiveness, and is protective against the otherwise detrimental effects of systemic iron overload

Figure 1-Figure Supplement 1: Cardiac and liver iron following dietary iron manipulation. Total elemental iron levels in heart and liver of C57BL/6 mice, under control conditions and after provision of low (Fe 5ppm) or high iron (Fe 5000ppm) diets from weaning for 6 weeks. *p=0.037 and 0.033 respectively relative to control heart, †p=0.010 and 0.005 relative to control liver. n=3. Data are represented as mean±SEM.

Figure 1-Figure Supplement 2: Furin regulation by iron. (A). Relative Furin mRNA in primary adult mouse cardiomyocytes under control conditions and following treatment with DFO or FAC. *p=0.004, 0.001 and 0.001 respectively relative to control at the respective timepoint. (B) Relative Furin mRNA in hearts of mice provided control diet or iron-deficient diet (2-5ppm) or iron-loaded diet (5000ppm) from weaning for 6 weeks. *p=0.015 relative to control diet. n=3. Data are plotted as mean±SEM.

Figure 1-Figure Supplement 3: Relative *Hamp* mRNA expression in cardiomyocytes following treatment with Furin inhibitor CMK. Relative *Hamp* mRNA expression in primary adult mouse cardiomyocytes under control conditions and following treatment with DFO or FAC, in presence or absence of Furin inhibitor CMK. n=3. Data are plotted as mean±SEM.

Figure 1-Figure Supplement 4: HAMP in supernatants of primary cardiomyocytes. HAMP protein was measured by ELISA in supernatants of primary adult cardiomyocytes, derived from *Hamp*$^{fl/fl}$ or *Hamp*$^{fl/fl}$*;Myh6.Cre*+ mice and cultured under control conditions or in presence of FAC or DFO. n=3. Data are plotted as mean±SEM.

Figure 1-Figure Supplement 5: Confirmation of HAMP antibody specificity. (A) Staining with HAMP antibody (Abcam ab30760) in liver and heart of C57BL/6 mice is completely abrogated by co-incubation with hepcidin-25 blocking peptide (Abcam ab31875). Scale bar=20μm. (**B)** Loss of HAMP staining in Hamp$^{fl/fl;}$*;Myh6.Cre*+ hearts (Figure 1F) is consistent with the antibody detecting HAMP1 and not HAMP2, because *Hamp*2 mRNA

expression is not altered in *Hamp*$^{fl/fl}$*;Myh6.Cre*+ mice relative to *Hamp*$^{fl/fl}$ controls, either with control diet or iron-deficient diet (6 weeks from weaning). *p=0.007 and 0.047 relative to *Hamp*$^{fl/fl}$ control under respective diet. n=3 per group. Values are plotted as mean±SEM. N.S=not significant.

Figure 1-Figure Supplement 6: HAMP detection by ELISA unaffected by FAC and DFO. HAMP standard from mouse hepcidin ELISA (E91979Mu, Uscn) was diluted either in the kit's own standard diluent, or in unconditioned growth medium alone, or containing 100µmol/L DFO or 500µmol/L FAC. ELISA was performed as per manufacturer's instructions.

Figure 3-Figure Supplement 1: Characterisation of *Slc40a1* C326Y$^{fl/fl}$;*Myh6.Cre*+ mice. Total mRNA was extracted from the liver and heart of an adult a *Slc40a1* C326Y$^{fl/+}$*;Myh6.Cre*+ mouse, reverse transcribed using primers for exon 7 of the *Slc40a1* mRNA transcript. Products were sequenced to confirm successful heterozygous expression of the C326Y transcript in the heart but not in the liver.

Figure 3-Figure Supplement 2: Elemental iron levels in total hearts of *Hamp*$^{fl/fl}$*;Myh6.Cre*+ mice, *Slc40a1* C326Y$^{fl/fl}$*;Myh6.Cre*+ mice and their respective controls at 3 months and 6 months of age. n=4 per group. Data are plotted as mean±SEM.

Appendix figure 1: Effect of Furin inhibitor on iron export in cardiomyocytes. Fe55 efflux measured in primary adult cardiomyocytes from Hamp *fl/fl* and Hamp *fl/fl;Myh6.Cre*+ mice following culture in control medium (-CMK) or medium containing Furin inhibitor (+CMK) for 2 hours. n=3. values are plotted as mean±SEM. *p=0.027. †p=0.024.

Appendix figure 2: Effect of genotype on hypertrophic response to iron-deficient diet. Heart/body weight ratio in Hamp$^{fl/fl}$;*Myh6.Cre*+ mice and littermate Hamp$^{fl/fl}$ controls provided a control diet (Fe 200ppm) or an iron-deficient diet (Fe 2-5ppm) from weaning for 6 weeks. n=5 per group, NS=not significant. *p=0.013, †p=0.04. Values are shown as mean±SEM.

Appendix figure 3: (A-C) Cine MRI measurements of LV lumen, at end-systole (LVES), end-diastole (LVED), and of ejection fraction (LVEF) in *Slc40a1 C326Y*KI/+ mice and +/+ littermate controls at 3 months (n=7 per group), 6 months (n=7 per group) and 9 months (n=7 per group) of age. Values are plotted as mean±SEM.

Appendix figure 4: Strategy for generation of *Hamp*$^{fl/fl}$;*Myh6.Cre*+ mice

A targeting vector was designed to introduce a floxed *Hamp* allele into mouse ES cells, with exons 2 and 3, which encode the majority of the peptide, flanked by LoxP sites. Further breeding with a C57BL/6 Flp recombinase deleter mouse allowed removal of the Neo cassette. Cardiac *Hamp* knockouts were then generated by crossing homozygous *Hamp*$^{fl/fl}$ animals with mice transgenic for *Myh6-Cre* recombinase, which is under the control of cardiomyocyte-specific Myosin Alpha Heavy chain 6 promoter.

Appendix figure 5: Strategy for generation of *Slc40a1 C326Y*$^{fl/fl}$;*Myh6.Cre*+ mice.

A targeting vector was designed to introduce a floxed *Slc40a1 C326Y* allele into mouse ES cells, containing mutant exon 7 and wild type and to delete simultaneously endogenous exons 7 and 8. Further breeding with a C57BL/6 Flp recombinase deleter mouse allowed removal of the Neo cassette. Cardiac *Slc40a1 C326Y* knock-ins were then generated by crossing homozygous *Slc40a1 C326Y*$^{fl/fl}$ animals with mice transgenic for Myh6-Cre recombinase, which is under the control of cardiomyocyte-specific Myosin Alpha Heavy chain 6 promoter.

Appendix figure 6: Additional images for HAMP and FPN staining. (A) Lower magnifications images (X10) for figure 1b. **(B)** Lower magnification images (X10) for figure 1f. **(C)** Higher magnification images (X40) for figures 3a and 3c.

Figure 2- source data 1: Source data file for figures 2i, 2j and 2k

Figure 3- source data 1: Source data file for figures 3j, 3k and 3l

Figure 4- source data 1: Source data file for figures 4a, 4b and 4c

Figure 1

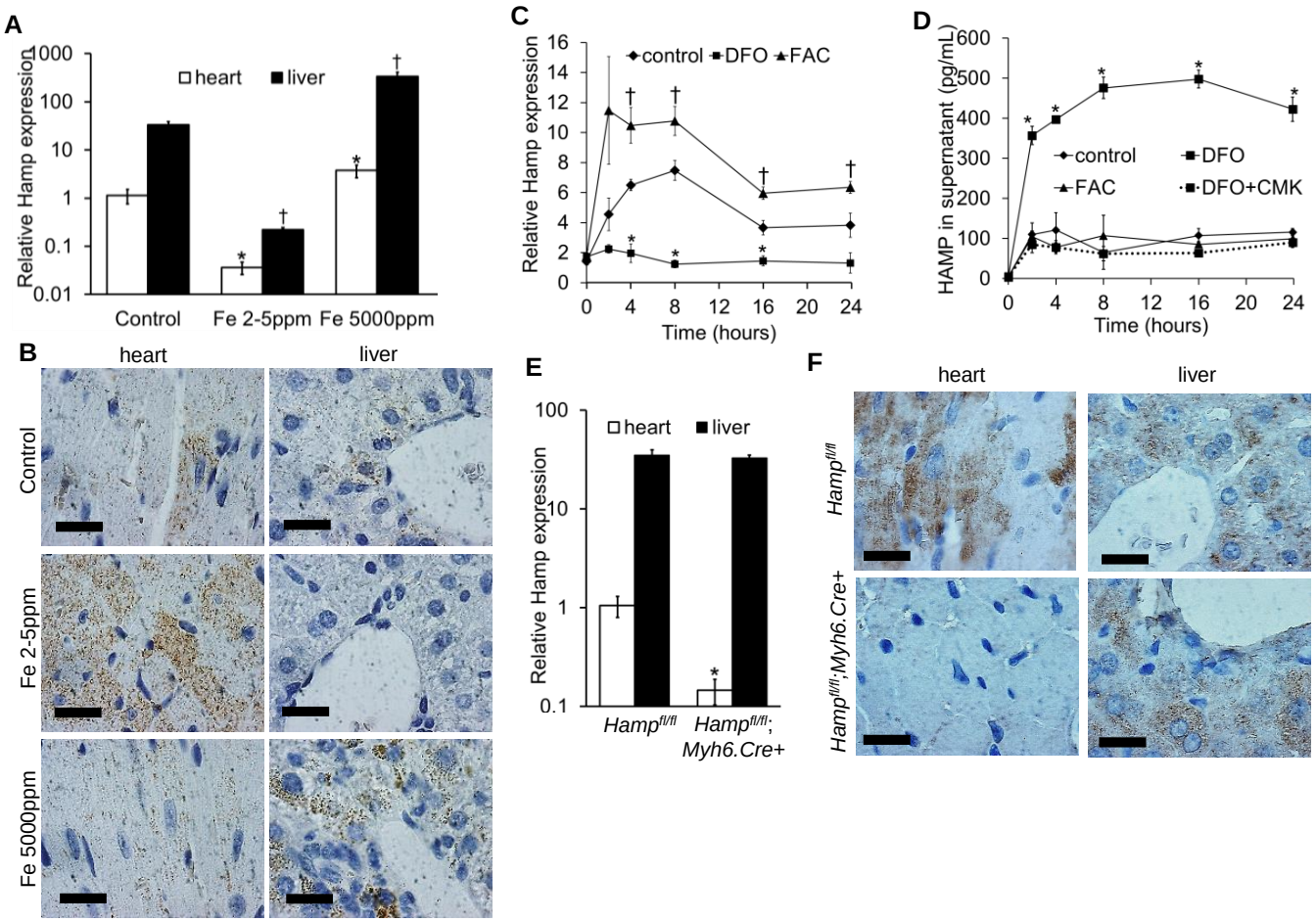
A
Relative Hamp expression
1000
100
10
1
0.1
0.01
heart
liver
Control
Fe 2-5ppm
Fe 5000ppm
B
heart
liver
Control
Fe 2-5ppm
Fe 5000ppm
C
Relative Hamp expression
16
14
12
10
8
6
4
2
0
control
DFO
FAC
0
4
8
12
16
20
24
Time (hours)
D
HAMP in supernatant (pg/mL)
600
500
400
300
200
100
0
control
DFO
FAC
DFO+CMK
0
4
8
12
16
20
24
Time (hours)
E
Relative Hamp expression
100
10
1
0.1
heart
liver
Hampfl/fl
Hampfl/fl;
Myh6.Cre+
F
heart
liver
Hampfl/fl
Hampfl/fl;Myh6.Cre+

Figure 2

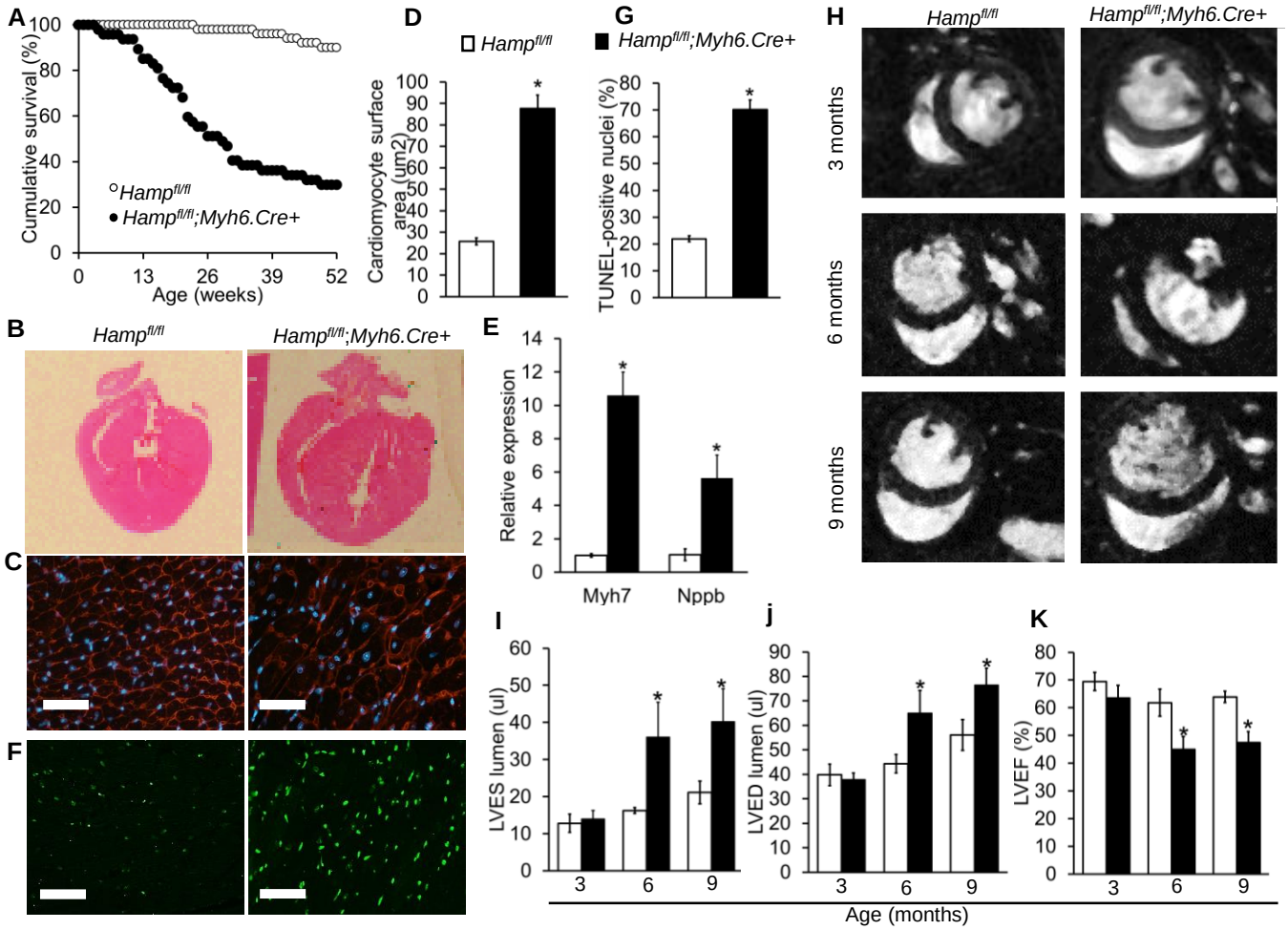
A
Cumulative survival (%)
Age (weeks)
Hampfl/fl
Hampfl/fl;Myh6.Cre+
D
Hampfl/fl
Cardiomyocyte surface area (um2)
G
Hampfl/fl;Myh6.Cre+
TUNEL-positive nuclei (%)
H
Hampfl/fl
Hampfl/fl;Myh6.Cre+
3 months
6 months
9 months
B
Hampfl/fl
Hampfl/fl;Myh6.Cre+
C
F
E
Relative expression
Myh7
Nppb
I
LVES lumen (ul)
j
LVED lumen (ul)
K
LVEF (%)
Age (months)

Figure 3

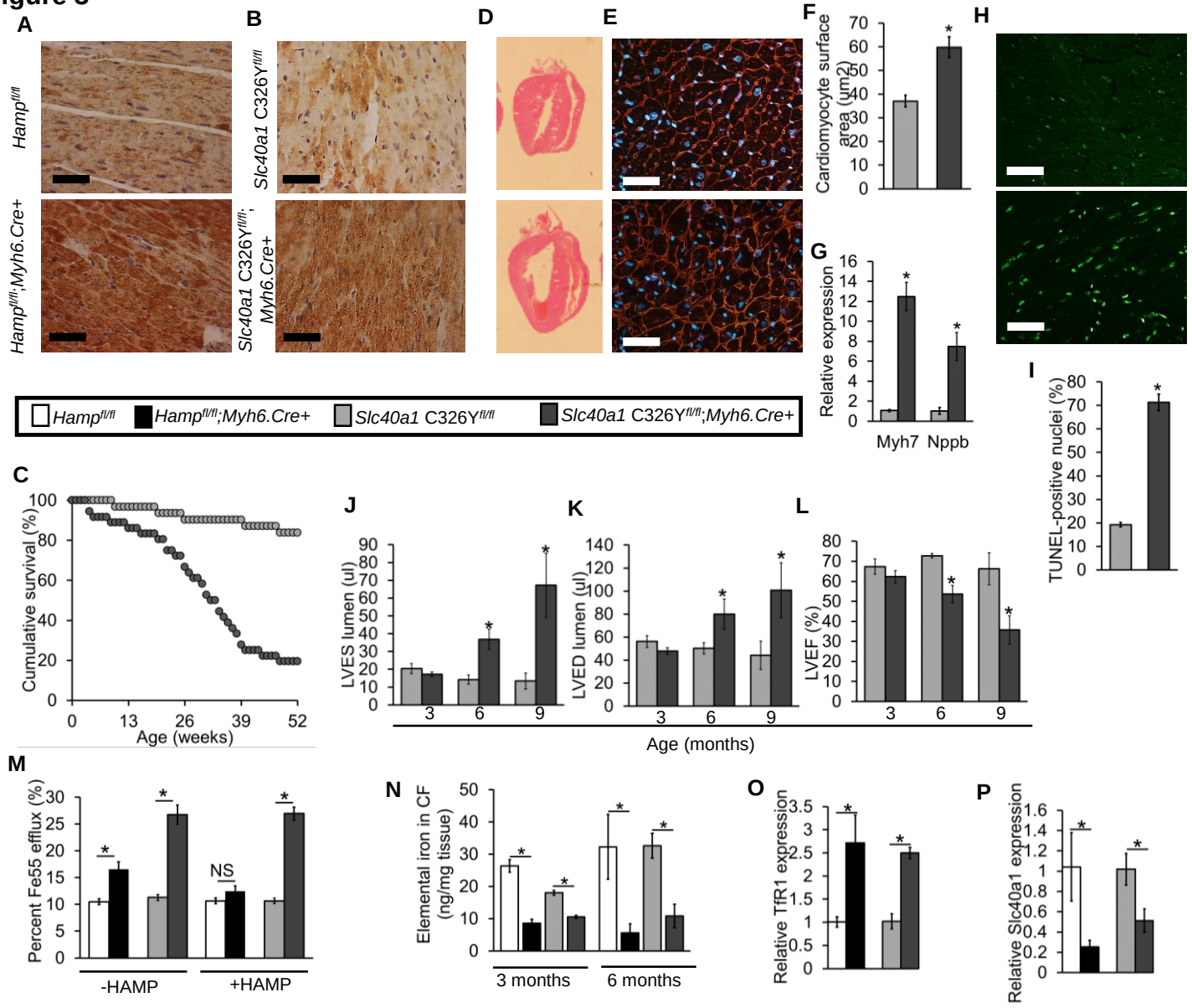
A
B
D
E
F
H
Hampfl/fl
Hampfl/fl;Myh6.Cre+
Slc40a1 C326Yfl/fl
Slc40a1 C326Yfl/fl; Myh6.Cre+
Cardiomyocyte surface area (um2)
Relative expression
Myh7
Nppb
Hampfl/fl
Hampfl/fl;Myh6.Cre+
Slc40a1 C326Yfl/fl
Slc40a1 C326Yfl/fl;Myh6.Cre+
I
TUNEL-positive nuclei (%)
C
Cumulative survival (%)
Age (weeks)
J
K
L
LVES lumen (ul)
LVED lumen (ul)
LVEF (%)
Age (months)
M
Percent Fe55 efflux (%)
NS
-HAMP
+HAMP
N
Elemental iron in CF (ng/mg tissue)
3 months
6 months
O
Relative TfR1 expression
P
Relative Slc40a1 expression

Figure 4

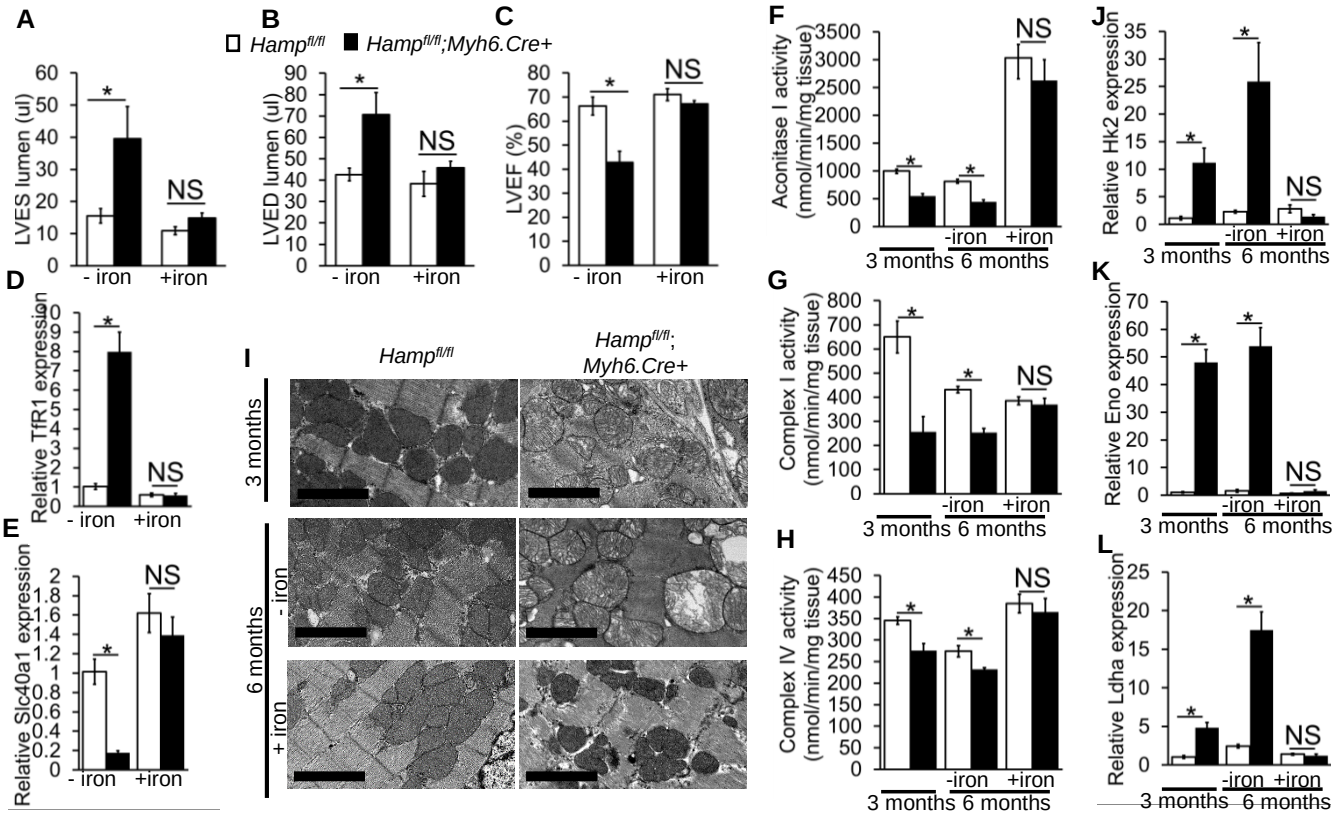
A
B
C
Hampfl/fl
Hampfl/fl;Myh6.Cre+
LVES lumen (ul)
LVED lumen (ul)
LVEF (%)
- iron
+iron
NS
D
Relative TfR1 expression
E
Relative Slc40a1 expression
I
Hampfl/fl
Hampfl/fl; Myh6.Cre+
3 months
6 months
- iron
+ iron
F
Aconitase I activity (nmol/min/mg tissue)
G
Complex I activity (nmol/min/mg tissue)
H
Complex IV activity (nmol/min/mg tissue)
-iron
+iron
3 months
6 months
J
Relative Hk2 expression
K
Relative Eno expression
L
Relative Ldha expression

Figure 5

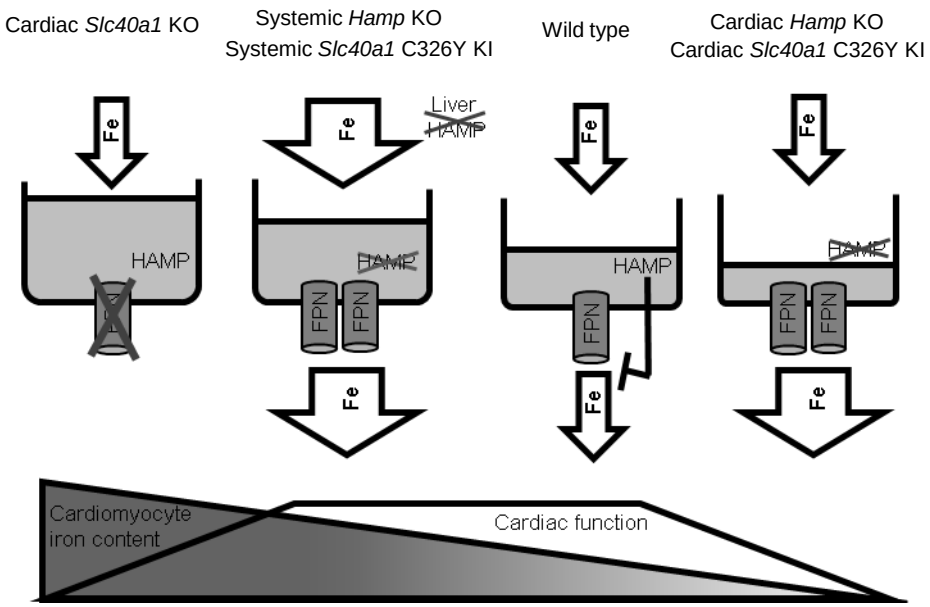
Cardiac *Slc40a1* KO
Systemic *Hamp* KO
Systemic *Slc40a1* C326Y KI
Wild type
Cardiac *Hamp* KO
Cardiac *Slc40a1* C326Y KI
Fe
HAMP
Liver
FPN
Cardiomyocyte
iron content
Cardiac function

Figure 1- Figure supplement 1

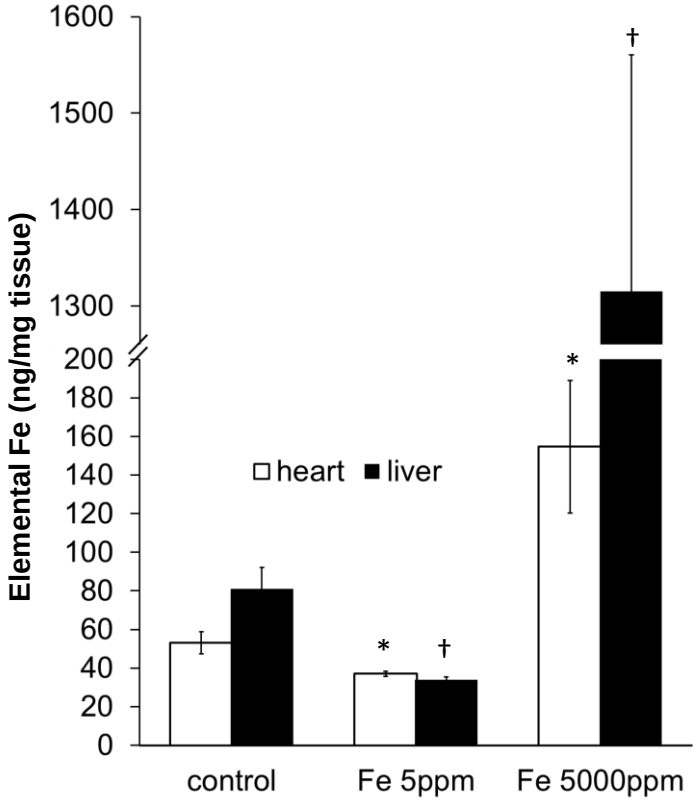

Figure 1- Figure supplement 2

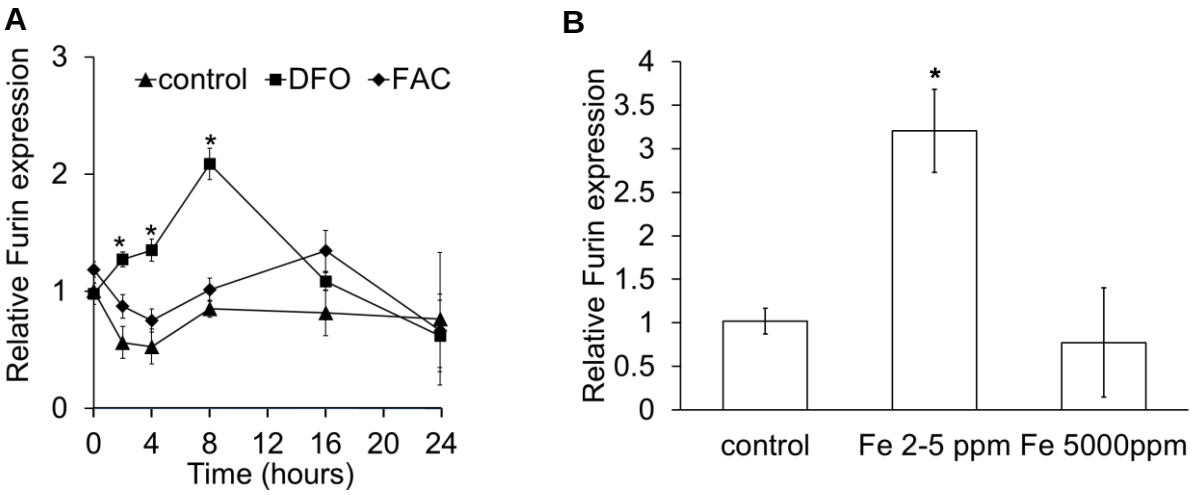

Figure 1- Figure supplement 3

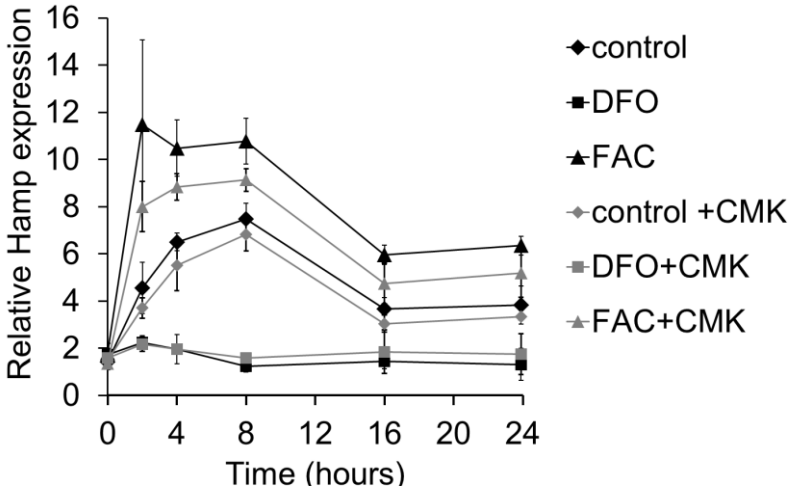

Figure 1- Figure supplement 4

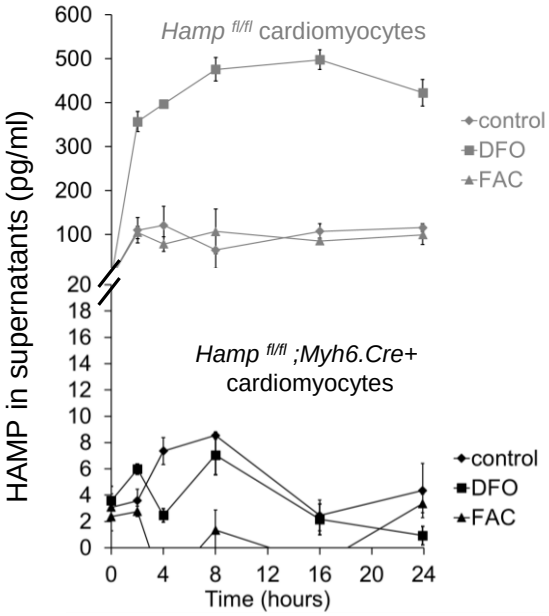

Figure 1- Figure supplement 5

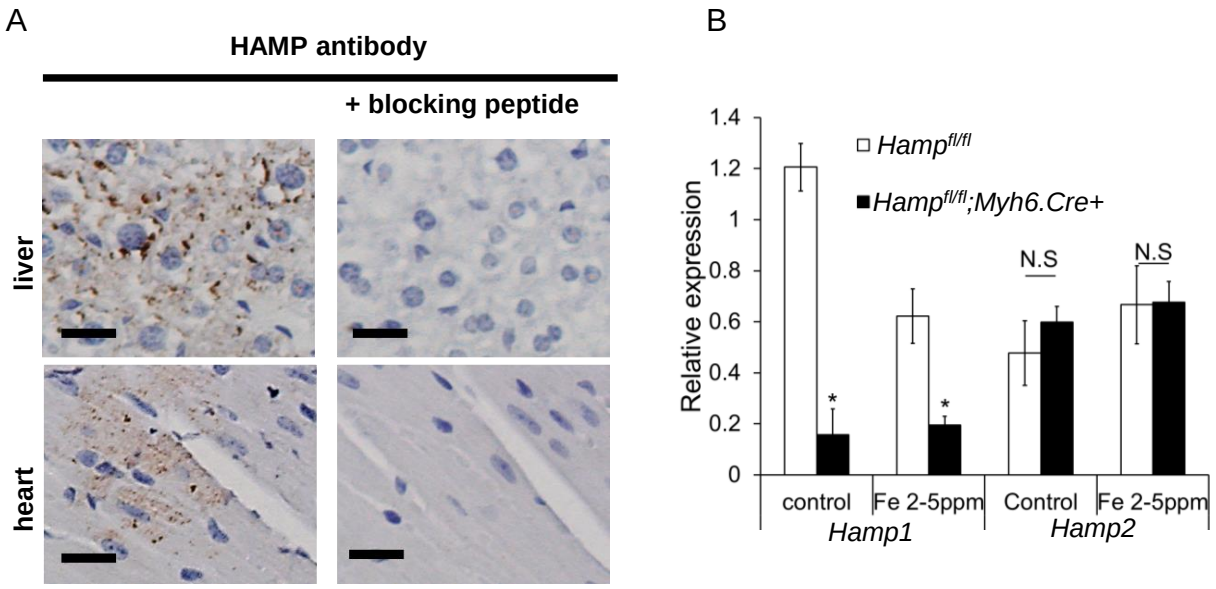

Figure 1- Figure supplement 6

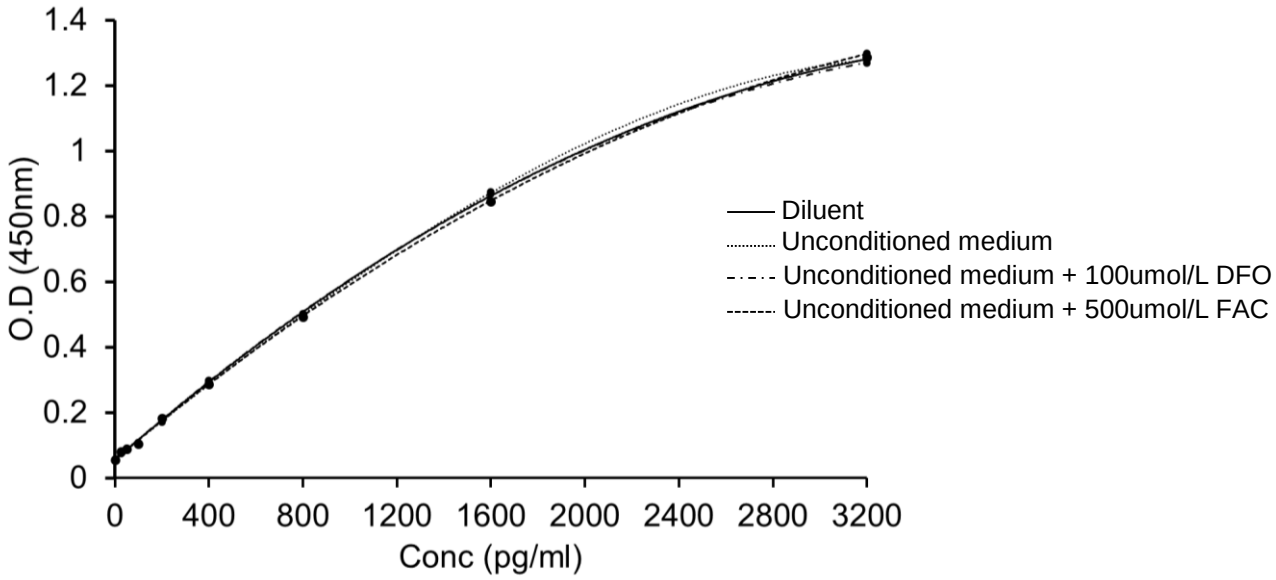

Figure 3- Figure supplement 1

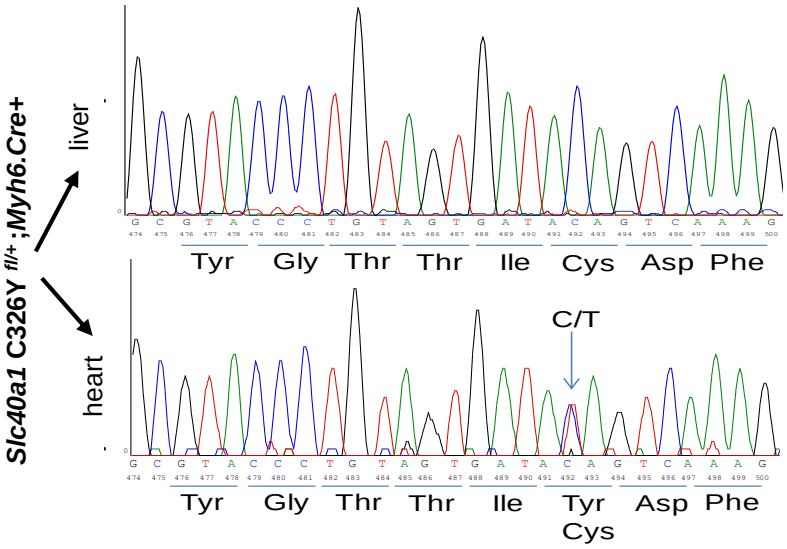

Figure 3- Figure supplement 2

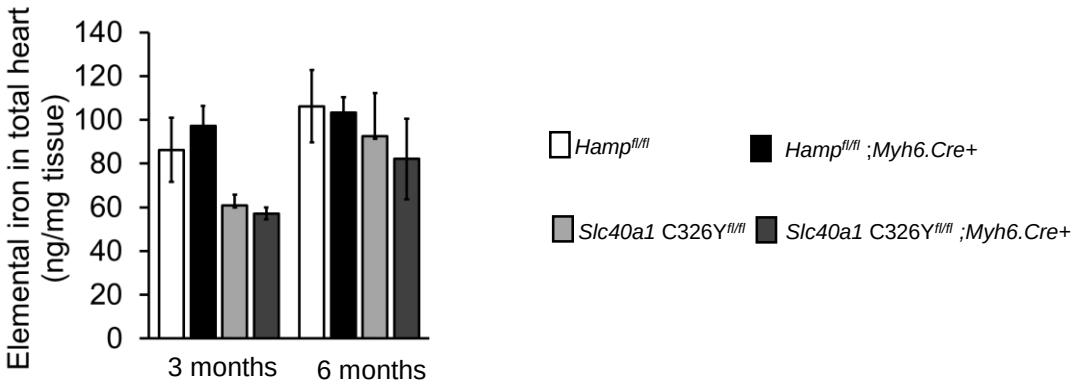

Appendix figure 1

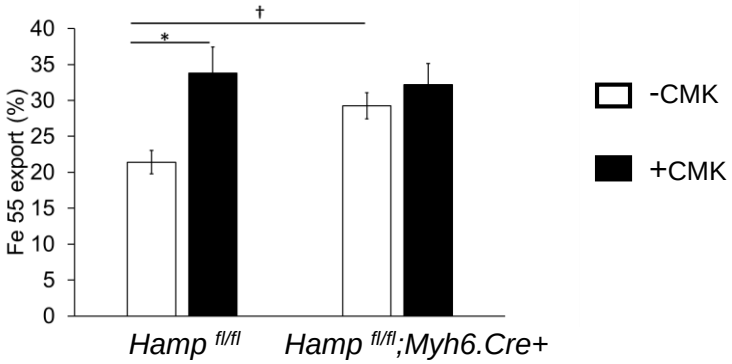

Appendix figure 2

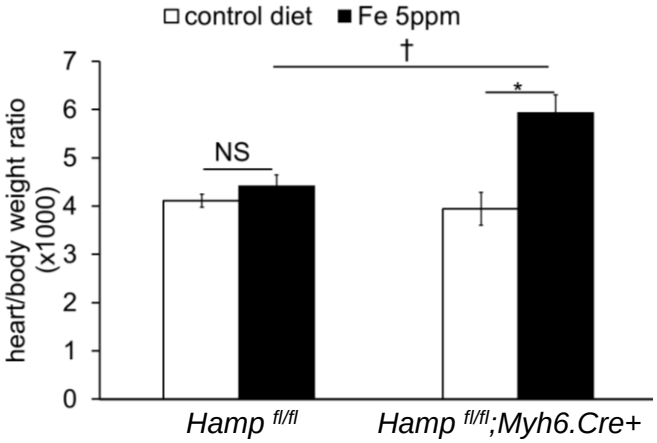

.

Appendix figure 3

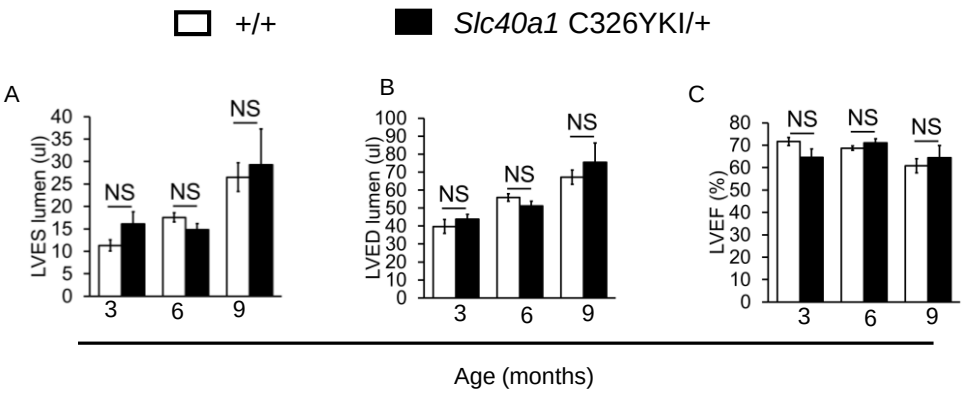

Appendix figure 4

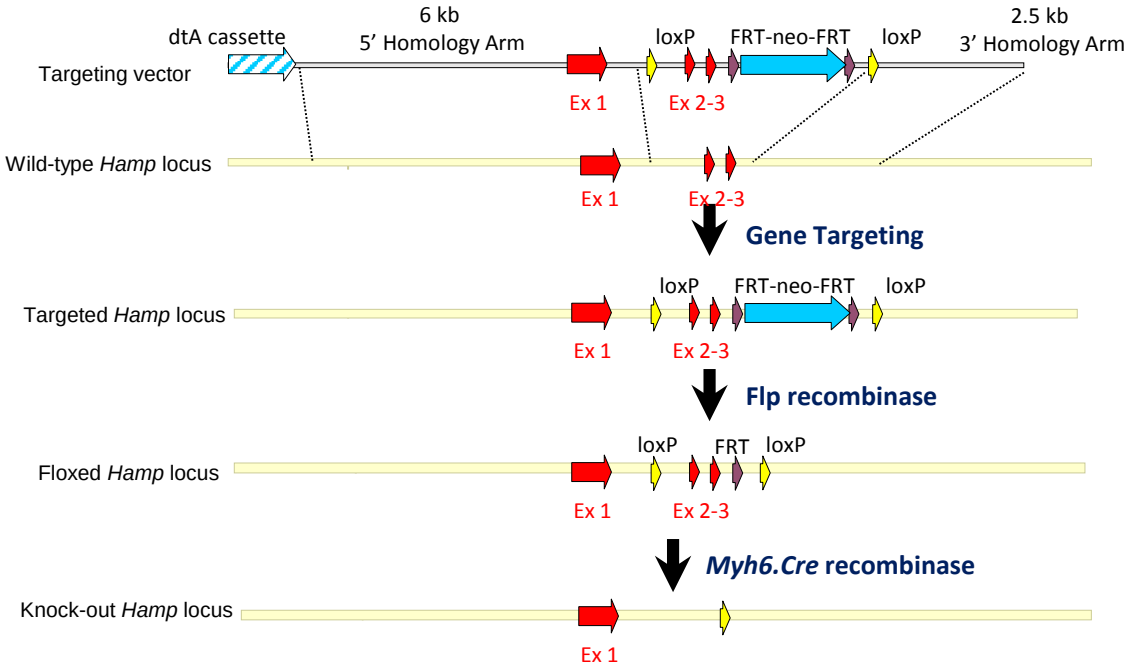

Appendix figure 5

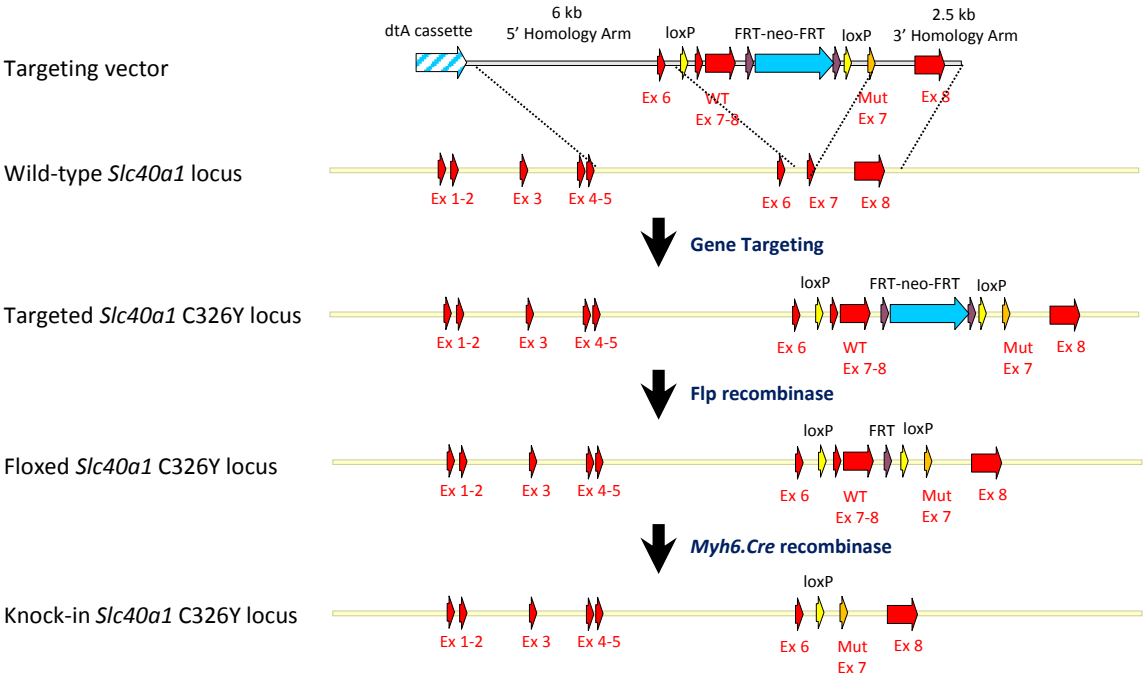

Appendix figure 6